Development of a Three-Dimensional Suspension Plasma Spray Coating Build-up Model

A Thesis

In

The Department

Of

Mechanical, Industrial and Aerospace Engineering (MIAE)

Presented in Partial Fulfilment of Requirements

For the Degree of Master of Applied Science at

Concordia University

Montreal, Quebec, Canada

April 2020

CONCORDIA UNIVERSITY

School of Graduate Studies

This is to certify that the thesis prepared

By: Behrad Kashfi Ashtiani

Entitled: Suspension Plasma Spray Coating Build-up Simulation

And submitted in partial fulfilment of the requirements for the degree of

Master of Applied Science (Mechanical Engineering)

Complies with the regulations of the University and meets the accepted standards with respect to originality and quality.

Signed by the final Examining Committee:

_____Marius Paraschivoiu_____Chair

_____ External Examiner

_____ Rolf Wuthrich _____ External to Program

_____ Marius Paraschivoiu _____ Examiner

_____ Examiner

_____Christian Moreau_____ Thesis Co-Supervisor

_____Ali Dolatabadi _____Thesis Co-Supervisor

Approved by: _____Martin Pugh_____

              Chair of Department or Graduate Program Director

_____ 2018   ____Mourad Debabbi_____ Dean of Faculty

Abstract

Suspension Plasma Spray Coating Build-up Simulation

Behrad Kashfi Ashtiani
Concordia University, 2019

During the last two decades, suspension plasma spray (SPS) coating methodology has drawn attention by showing a capacity to achieve a broad range of coating characteristics. Enormous efforts have been made to find the influential parameters on the SPS coating microstructure. However, due to the high computational costs and the complexity of the process, most of the studies have an experimental foundation. Regarding the high expenses of empirical investigations and time-consuming processes involved, such as setting up, sample preparation, etc., a simulation tool giving an approximation of the final coating properties is essential more than ever. A Simulation tool can provide also complementary information that help us better understand the coating microstructures obtained experimentally.

This study aims to provide a tool to simulate SPS coatings build-up by applying both computational fluid dynamics (CFD), and an in-house developed model in MATLAB. The model can be used generally for SPS coating build-up simulations and is not limited to the studied problem. The framework was formed around a previously developed model with significant enhancements regarding the accuracy and computational cost.

Two different approaches were followed in modeling particle deposition, considering the particle flattening process or deposition as a non-deformed particle. Results from both models offer promising trends capturing various coating microstructures already reported in the literature and predicting the effects of substrate geometry on the coating evolution. However, the porosity level

and deposition rate are overestimated due to the assumptions made and the lack of data regarding

the deposition efficiency based on the particle characteristics, respectively.

Table of Contents

List of Figures

List of Tables

List of Abbreviations

Abbreviations	Meaning (unit)
APS	Atmospheric plasma spray
SPS	Suspension plasma spray
YSZ	Yttria-stabilized zirconia
CFD	Computational fluid dynamics
EB-PVD	Electron beam physical vapor deposition
TBC	Thermal barrier coating
PVD	Physical vapor deposition
MC	Monte Carlo
MD	Molecular dynamics
FR	Flattening ratio

List of Symbols

Symbol	Meaning (unit)
St	Stokes number
μ_g	plasma gas dynamic viscosity
μ_l	liquid carrier kinematic viscosity
Re	Reynolds number based on droplet size and liquid carrier characteristics
x_p	Location of a particle regarding x-axis
y_p	Location of a particle regarding y-axis
z_p	Location of a particle regarding z-axis
v_{xp}	Velocity vector regarding x-axis
v_{yp}	Velocity vector regarding y-axis
v_{zp}	Velocity vector regarding z-axis
d_p	Particle diameter
T_p	Particle temperature
N_p	Number of particles in a parcel
x_r	Random value added to landing position regarding x-axis
y_r	Random value added to landing position regarding y-axis
L_{ave}	Gap space
M_{inj}	Sum of the mass of landing particles in a specific torch position
m_p	Mass of particle

Δt_{rep}	Database representative time
ρ_p	Density of particles
Δt_{land}	Interval for the particle to move 100 μm in z-axis
X_{land}	Deposition location of the particle regarding x-axis
Y_{land}	Deposition location of the particle regarding y-axis
$\bar{d}$	Mass average of landing particles on the substrate for a specific torch position
$\bar{m}$	Average mass based on $\bar{d}$
D_s	Distance between a deposited particle and trace-line of the investigated flying particle
d_s	Diameter of the investigated deposited particle
FR	Flattening ratio
a	Long diameter of the splat
b	Short diameter of the splat
b_{max}	Maximum value possible for the shorter diameter of the splat
γ	Flying particle trace line angle relative to the substrate level

Chapter 1.   Introduction

1.1. Background and motivation

Coating is a process in which a covering material is applied onto the surface of an object, usually referred to as the substrate. Thermal spray is one of the numerous coating technics in which melted material is sprayed onto the substrate to improve or restore the surface of a solid material. Thermal spray can provide resistance to wear, erosion, cavitation, corrosion, abrasion, or heat. Thermal barrier coatings for protection of superalloys in gas turbines, passive and active (cathodic) protection in corrosive environments, and wide-ranging hard metal cermet and advanced alloy coatings in case of abrasive, sliding, erosion or wear are amongst the most prominent applications [1].

All thermal spraying techniques involve small softened particles which deposit onto a prepared surface to form a continuous coating. High kinetic and thermal energy makes the particles to flatten or splat and form a bond with underlying particles producing a cohesive coating of successive layers. Understanding how the spray parameters influence the coating microstructure is critical in optimizing its properties, such as porosity content, hardness, and adhesion.

Plasma spray is a subcategory of thermal spray in which the coating material is injected into the plasma flame to be heated to high temperature and accelerated towards the substrate. What distinguishes the plasma spray process from other technologies is its capacity in processing a wide

variety of materials, metallic and refractory materials at atmospheric pressure. The most conventional method in plasma spray is the atmospheric plasma spray (APS) to deposit thick coatings (from hundreds of micrometers to a few millimeters) with a high deposition rate. Enhancing the APS coating properties necessitates the deposition of finer particles, while there are limitations in this regard. That problem was circumvented by dispersing the coating material or feedstock in a solvent and injecting the resulting suspension into the plasma flow, which is known as the suspension plasma spray (SPS) method.

SPS is a relatively new coating method in plasma spray, which has shown high potential to provide diverse microstructures with a broad range of porosity. This diversity in properties has drawn the researchers' attention to find the influential parameters controlling the coating characteristics. Despite tremendous efforts regarding the experimental aspect of the subject, the numerical investigations seem to be limited. Considering the burden of high expenses by empirical studies, a reliable simulation tool can lead to huge savings and help the technology getting widespread.

1.2. State of the art techniques to SPS coating build-up simulation

SPS is a relatively new coating technique, which is opening its way through some industrial applications in aerospace, energy, environment and electronic sectors. Numerous experimental studies have led to a better understanding of the process and influencing parameters controlling the coating microstructure. However, those studies have a qualitative approach, while tailoring the coating microstructure necessitates having a reliable simulation tool.

To the best knowledge of the author, the only published SPS coating build-up modelling study is the one from Ghafouri Azar [2], where a database of particles, at 100 μm distance to the

2

substrate, was applied to fill a uniform gridded computational domain. Therefore, all the particles were assumed to have the same shape and size conformal to the grid, and the flattening process considered to be negligible. By making some simplifications, the deposition location of each particle was computed, leading to the formation of coating.

Despite significant progress made, several limitations were preventing the model from being applicable, above all the unaffordable computational cost. A critical review of that work is provided in section 2.4.

1.3. Objectives

The purpose of this study is defined as:

Developing a SPS coating build-up model, that predicts various coating microstructural features observed experimentally in SPS-deposited coatings. The software must be computationally affordable and provide a distinguishable picture of the coating microstructure including features such as column density and size.

1.4. The scope of work and limitations

The developed simulation tool is supposed to be applicable generally in modeling any SPS coating build-up problem. Any substrate shape can be introduced as the input and different theories regarding the splat geometry could be investigated. The challenges of this work are the development of a reliable model regarding the deposition process, and also making the simulations computationally affordable.

The presented results are based on a study [3] in the simulation of injecting yttria-stabilized zirconia (YSZ) into 3MB Oerlikon-Metco torch. It should be mentioned that this case provided

3

the only set of data for the author. Therefore, validation was performed just based on some observations made in experimental investigations reported in the open literature and some fundamental theories.

1.5. Thesis outline

This work was performed to develop a tool for simulating SPS coating build-up based on input data from numerical analysis of the flow by computational fluid dynamics (CFD) methods. This thesis is divided into five chapters, which a brief description of each is as follows:

Chapter 1 presents the background and motivations to develop this work. State-of-the- art techniques to simulate the coating build-up are explained. The objectives and scope of the work are defined as well as this thesis is outlined.

Chapter 2 presents a brief review of the thermal spray processes and methodologies, focusing on SPS applications and critical factors affecting its coating structure, followed by a summary of numerical methods used to simulate of coating build-up in different coating processes.

Chapter 3 presents the procedure and methods applied in the development of the simulation tool.

Chapter 4 presents the results of applying the developed simulation tool for some numerical investigations.

As a final point, the conclusion of the work and future research is discussed in Chapter 5.

Chapter 2.   Literature Review

In this chapter, the thermal spray processes and methodologies are described focusing on suspension plasma spray (SPS) applications and critical factors affecting its coating structure. In the following, a summary of some numerical methods in simulation of different coating technics is reviewed.

2.1. Thermal spray

Thermal spray coatings have been widely used in applications such as wear resistance, corrosion resistance, thermal protection, bioactivity, dielectric properties, etc. [4]. The process not only creates coating of unique microstructure, but also offers a wide choice of materials and processes that have a reduced the impact on the environment when compared to some conventional processes [5]. Thermal spraying is a process in which the coating material, known as feedstock, heated by a spray torch, is propelled towards a surface known as substrate. The heated feedstock forms droplets or particles, which are in a molten or semi-molten condition when impacting the substrate forming splats. The accumulation of those solidified droplets creates the coating. Coating materials available for thermal spraying include metals, alloys, ceramics, plastics, and composites, which are heated by combustion or electrical arc discharge as the sources of energy. A schematic of the process is shown in Figure 2-1.
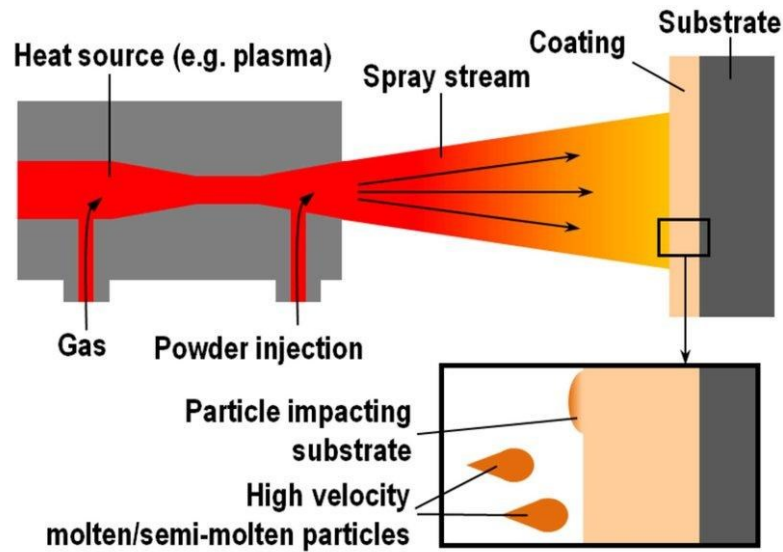
Figure 2-1: Schematic illustration of thermal spray process [6]

Plasma spray is one of the several variations of thermal spray in which feedstock is introduced into the plasma jet, induced by an electric discharge between electrodes, emanating from a plasma torch. Then the molten droplets flatten, impacting the substrate and solidify to deposit with splat with dimensions ranging from a few hundred nanometers to above 100 μm. This variation in size presents various coating microstructures with significantly different properties. Generally, the smaller and lighter particles are highly deviated by plasma jet compared to larger and heavier ones. The schematic of the plasma stream and particle interaction is shown in Figure 2-2. As can be seen, the plasma flow gets deviated facing the substrate and forms a boundary layer due to the viscous effects near the surface. Theoretically, the light particles follow closely the streamflow and never impact the substrate.
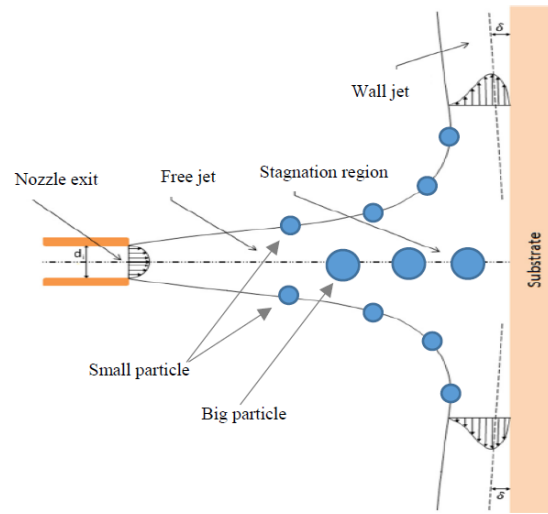
Figure 2-2: Schematic of a typical impinging gas-jet system [7]

Figure 2-3 illustrates the results of a numerical simulation investigating variations in the vertical velocity of droplets of different sizes through the interaction with plasma flow. It can be seen that the larger particles have higher normal impact velocity when compared to smaller particles, which get highly deviated by the plasma flow. Therefore, as the flying particles get smaller, plasma stream and viscosity play a more critical role in their trajectory.
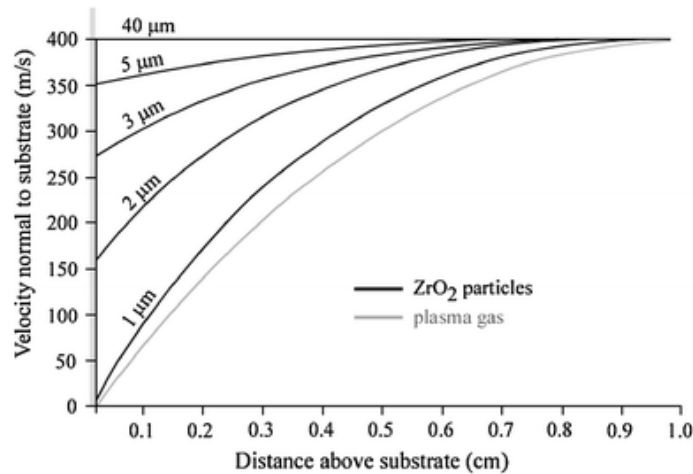
Figure 2-3: Changes in normal velocity of particles of different sizes impinging on a substrate [8]

The problem could be quantified by calculating Stocks number for the in-flight particles:

$$St = \frac{\mu_g}{\mu_l}\frac{1}{Re}$$

7

as μ_g, μ_l, and Re are plasma gas dynamic viscosity, liquid carrier kinematic viscosity, and Reynolds number based on droplet size and liquid carrier characteristics, respectively. Depending on the in-flight particle sizes, different coating microstructures could be obtained.

Regarding the particle size, plasma spray technic has two methods with different length scales. In atmospheric plasma spray (APS) as one of plasma spray subsets, the feedstock is injected by a carrier gas through the plasma flow, and particle size ranges from 20 to 200 μm. A schematic of the APS process is shown in Figure 2-4.
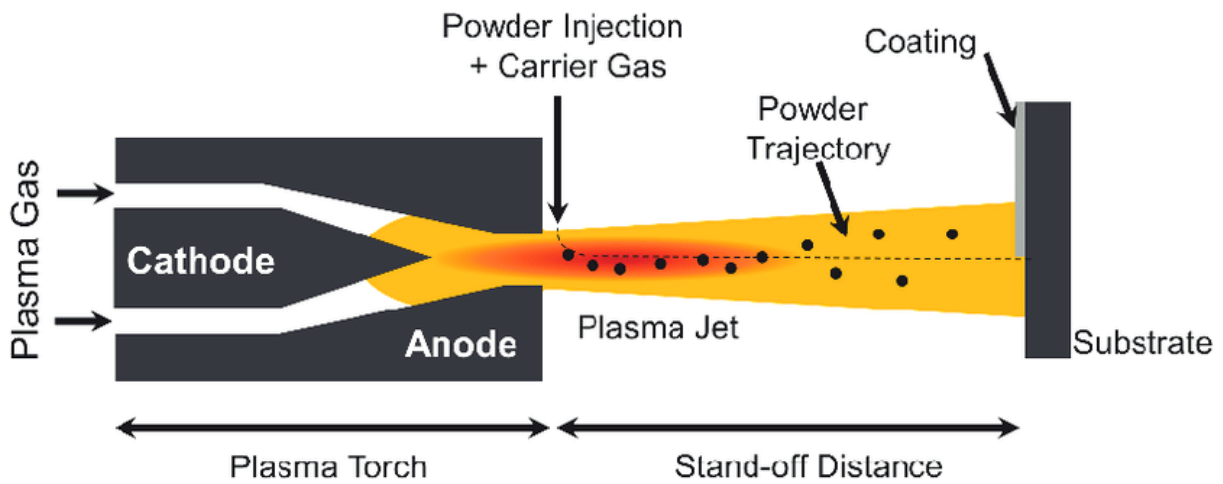
Figure 2-4: Schematic of APS process [9]

Regarding the characteristic length of the particles in APS and the theories described around the interaction of plasma flow and flying particles, the particles would not be perturbed by the plasma stream and will have a nearly perpendicular deposition. Therefore, the particles make relatively large splats and build-up layer by layer to form a typical lamellar microstructure, as shown schematically in Figure 2-5 [10].
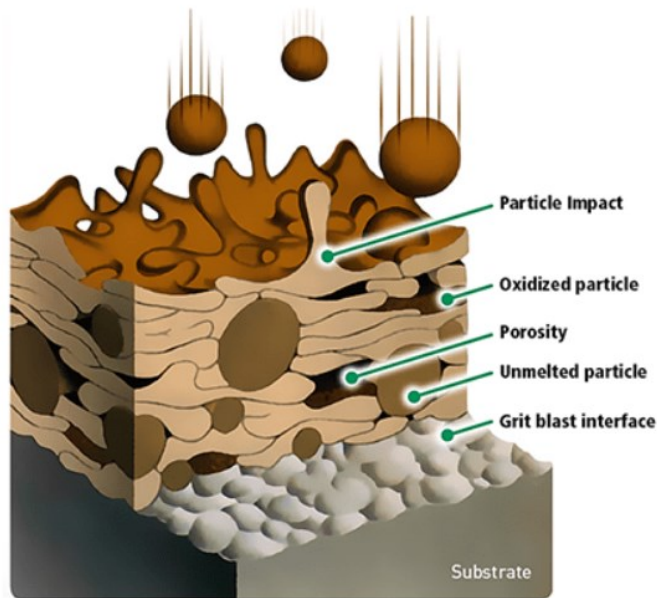
Figure 2-5: A typical microstructure seen in APS coatings [10]

It should be mentioned that the coating properties improves by deposition of coatings with finer microstructure, improving mechanical stresses [11]. However, APS has limitations regarding the feedstock characteristic diameter. As the size reduces, the carrier gas flow rate must be increased to be able to inject the particles through the plasma flow, which also increases the injection mass flow. For feedstock size of less than 5 μm, the injection would perturb the plasma flow, making it difficult to get a stable particle flow, leading to clogging problems, affecting the deposition efficiency and the coating quality [12].

Suspension plasma spray is a new version of APS, enabling spraying of fine feedstock particles (100 nm-5 μm diameter) [13]. In this method, the feedstock particles are dispersed in a liquid forming a suspension. By suspending powder in a fluid, typical feeding problems are circumvented, allowing the deposition of fined microstructures using finer powders. Generally, the dimension of the in-flight feedstock particles is in the range of a few hundred nanometers to a few micrometers. A schematic of the process is provided in Figure 2-6.
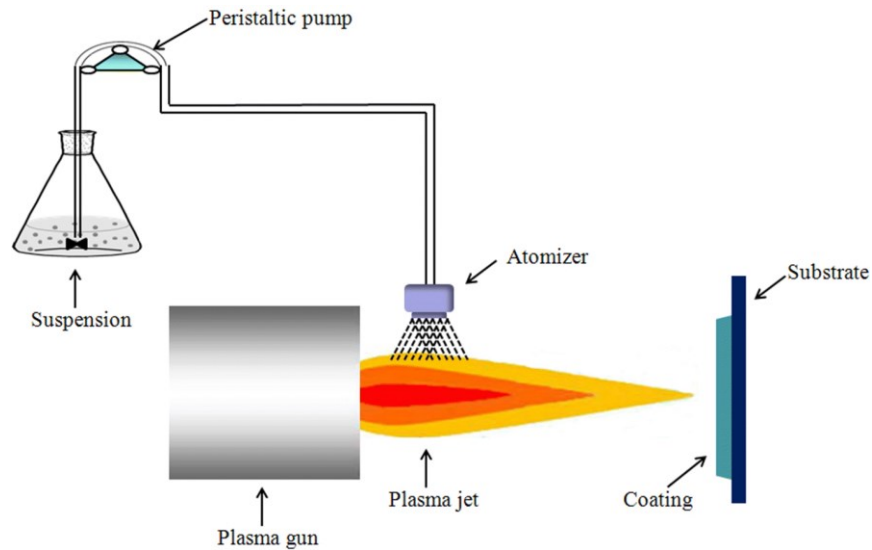
Figure 2-6: Schematic of SPS process [14]

The interaction of plasma jet and injected solution in SPS leads to the atomization of the droplets. The suspension droplet evolution in the plasma jet is shown in Figure 2-7. When large droplets are injected through the plasma flow, the drag forces coming from droplet-plasma interaction yield shear deformation, and therefore a break-up of the droplet. Then the solvent liquid is evaporated, which takes a time about two orders of magnitude larger than that of atomization (0.3 μs) [15]. After the evaporation, the sintering of some fine solids occurs, followed by the melting and impact on the substrate.
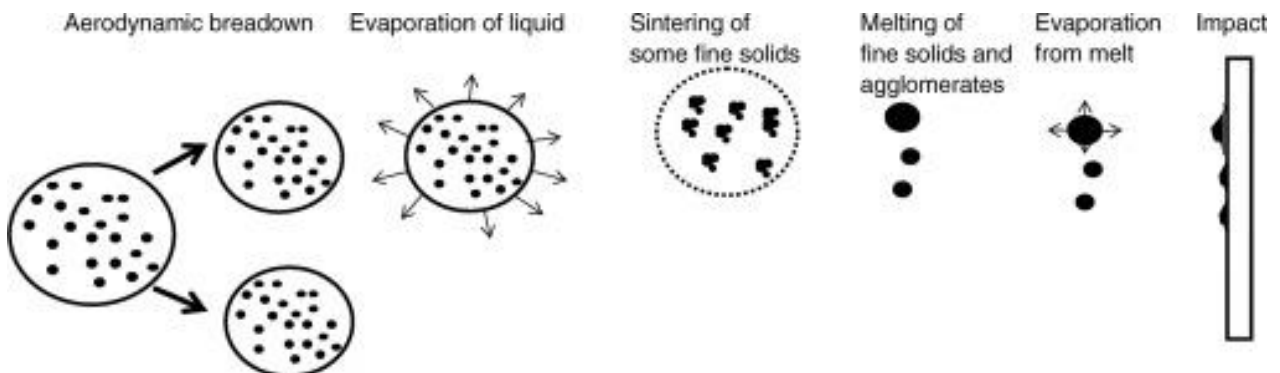
Figure 2-7: Transformation of suspension droplet in the plasma jet [15]

Due to the relatively small particle size in SPS, the coating microstructure gets so sensitive to any change in plasma flow, as it can highly influence the properties of depositing particles.

10

Many factors are influencing SPS coatings characteristics such as plasma gas, liquid carrier material, injection rate, torch power, suspension density, etc., which make it challenging to optimize coating microstructure. Features such as turbulent flow, interaction of three phases of materials including plasma, melting and solidification of droplets, and plasma flow fluctuations are just a part of the complexity of the problem. SPS process might lead to microstructures with segmented vertical cracks or column-like structures that imitate strain-tolerant APS or electron beam physical vapor deposition (EB-PVD) coatings, respectively [16]. Some variations of SPS columnar microstructure are shown schematically in Figure 2-8.
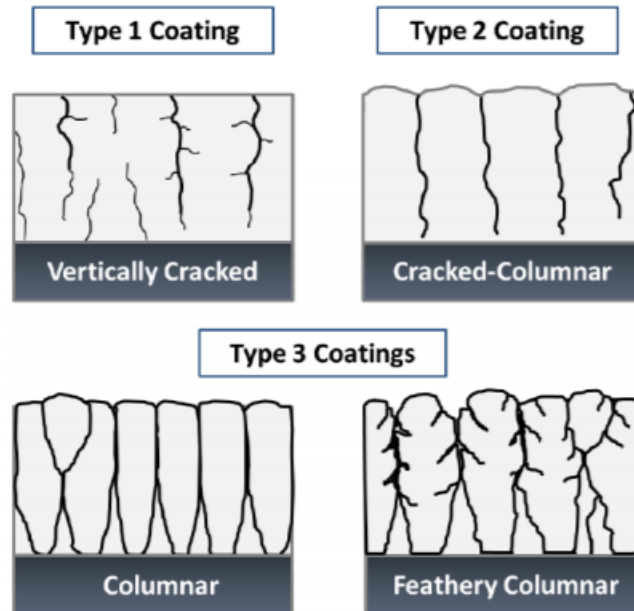
Figure 2-8: Schematic of different microstructures manufactured by SPS [17]

One of the exciting features of SPS coating is the capability of producing a columnar microstructure, enabling the relief of thermal stresses and a longer lifetime of the coating. Therefore, numerous studies have been devoted to identifying the creation and influencing parameters on the SPS columnar microstructure.

VanEvery et al. [18] justified the formation of SPS coating build-up based on particle trajectory by the so-called "shadow effect." As mentioned earlier, light particles are theoretically following the jet stream and therefore have a path almost parallel to the substrate close to its surface, while larger particles cross the streamlines and impact with a more perpendicular trajectory. The case (a) in Figure 2-9 shows the microstructure formed by very tiny particles with a trajectory almost parallel to the substrate. In this situation, substrate asperities make a high shadow effect and prevent piling particles in their sides. Case (b) describes relatively larger particles in which the difference in momentum makes them deviate from plasma trace-line at a specific turning angle. The horizontal velocity vector is still dominant but cannot prevent piling the particles adjacent to the asperities. Case (C) is for massive particles in which gas flow around the substrate does not influence their trajectory, and the impact is nearly normal. In this type, the gap between asperities can be filled, and we see a uniform piling of the particles on the substrate.
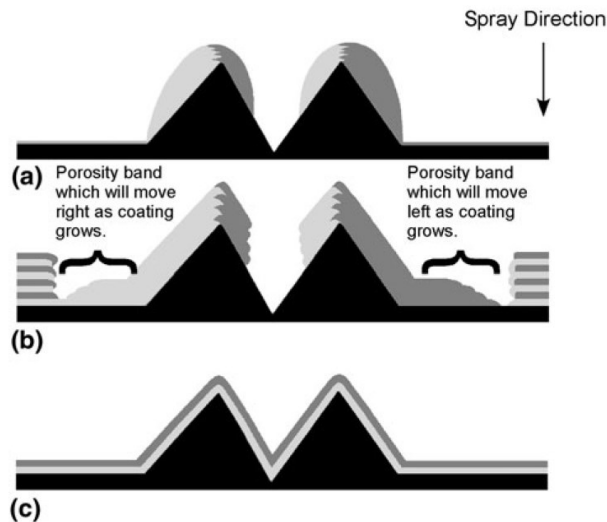
Figure 2-9: Schematics illustrating the deposition characteristics occurring on and away from substrate surface asperities [18]

SPS columnar microstructure could be justified based on the shadow effect theory. Due to the small size and therefore shallow trajectory of in-flight particles, the substrate asperities act

more efficiently regarding coating build-up, which makes the stems, and form the columns. Those asperities could even be created randomly on smooth surfaces by deposited particles.

SPS has found applications in several domains. For example, in solid-oxide fuel cells, SPS was used for producing highly porous coatings with fine pore sizes needed as electrodes [19]. However, the primary use of SPS is in the production of thermal barrier coating (TBC) in gas turbines. Demand for higher efficiency in gas turbine engines has led to a continuous increase in the gas inlet temperature by applying TBCs.

Bernard et al. [20] compared the conductivity of TBCs produced by APS, SPS, and Electron-beam physical vapor deposition (EB-PVD) techniques. Three different types of SPS structures was achieved by playing with the influential variables to reach different intercolumnar spaces. Heat diffusion mechanisms are compared in Figure 2-10.
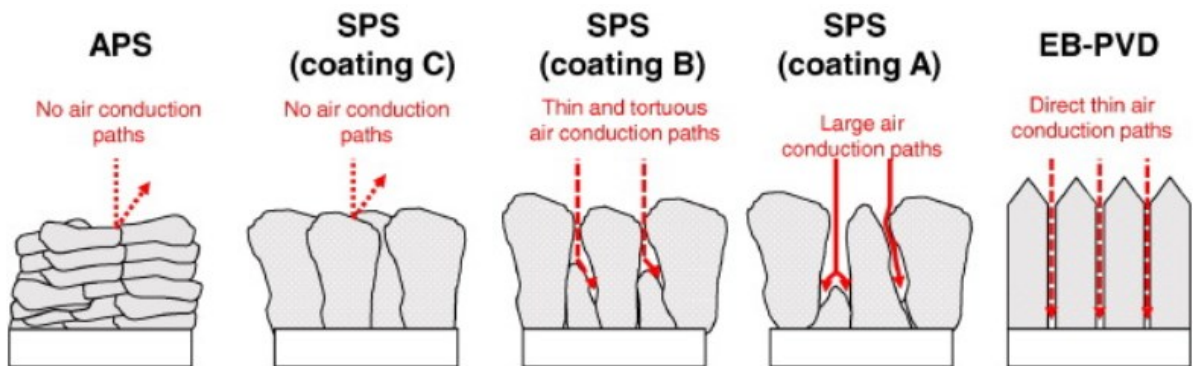
Figure 2-10: Air conduction consideration for coatings performed by SPS, APS and EB-PVD [20]

The thermal conductivity of yttria-stabilized zirconia (YSZ) TBCs manufactured by SPS, APS, and EB-PVD has been compared, as shown in Figure 2-11. All three SPS cases showed lower thermal conductivity compared to EB-PVD, and two of them had conductivity even better than APS. EB-PVD made of very dense columns, provided a poor heat conduction resistance, as the tiny intercolumnar gaps allowed the hot gas to diffuse directly. In SPS, the columns are not dense,

and nano-size pores make obstacles to heat conduction. Additionally, controlling the intercolumnar space made it possible to improve the TBC performance of these coatings.
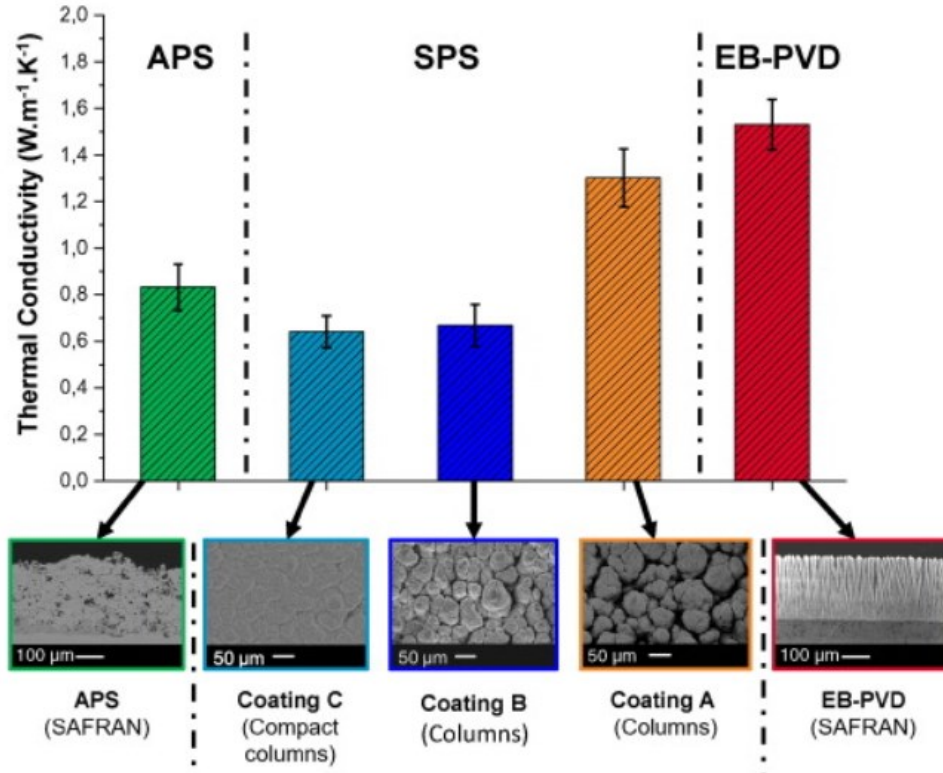
Figure 2-11: Thermal conductivities at 25 °C of YSZ samples performed by SPS compared to YSZ obtained by APS and EB-PVD [20]

In APS, due to lower porosity as compared to SPS cases, the coating shows a higher thermal conductivity. However, as the direct heat diffusion seen in columnar microstructures is absent, the APS coating showed a better thermal insulation property as compared to one of the SPS cases. Nonetheless, APS morphology does not have a mechanism to release the stresses of high temperature gradient. Phonons scattering mechanisms are shown in Figure 2-12.
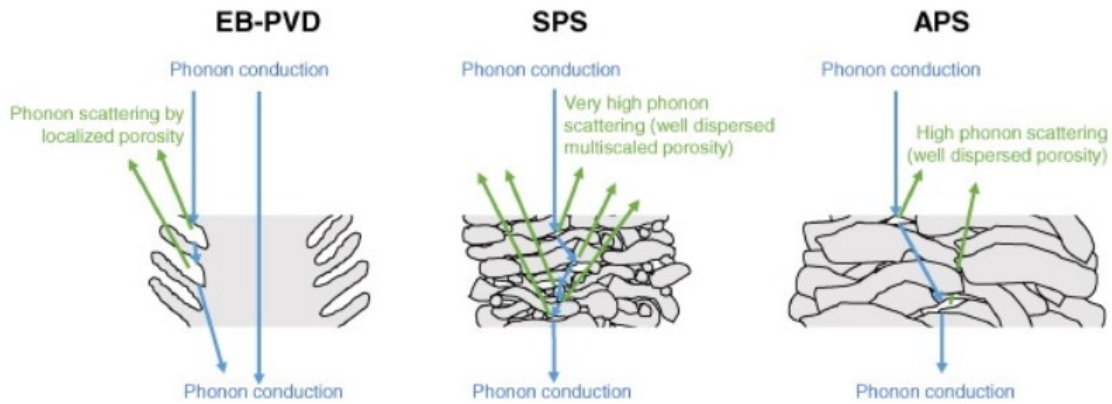
Figure 2-12: Phonon scattering for different configurations (EB-PVD, SPS and APS) [20]

SPS has shown high potential to improve TBC characteristics. However, SPS necessitates more energy per deposited mass comparing to conventional powder spraying due to the energy needed for vaporizing the liquid carrier requiring the use of high-enthalpy gas mixtures. It should be mentioned that due to the relatively small size of the SPS particles, the re-solidification might happen which could be prevented by limiting the stand-off distance which in turn leads to higher heat transfer to the substrate and therefore need to higher cooling preparations and probably limitations regarding the applicable substrate materials.

In the next section, a review is made on some studies regarding the influential parameters controlling SPS coating microstructure.

2.2. Review on SPS publications

Previously, it was noted that the key parameters controlling the plasma spray coating build-up, are the size and state of the in-flight particles. Unfortunately, the number of parameters influencing particle size is vast. Feedstock size, suspension concentration, liquid solvent, carrier gas, injection rate and angle, plasma gas mixture, torch design, applied power, environmental condition, and stand-off distance are just a number of those variables. Therefore, optimizing the

15

SPS coating microstructure requires an in-depth investigation of each of those variables. In this section, a very brief review of some of those studies is presented.

The carrier liquid is proven to have a significant influence on the first breakup [19]. Still and superposed images of different liquids injection into the same plasma are shown in Figure 2-13. As can be seen, atomization has happened at an earlier stage of penetration from left to right [21]. It seems this comes from the water droplets to be less susceptible to plasma drag influence. The same observations were also reported by Curry et al. [22]. From the other side, spray cones coming from the superimposed image show the opposite trend as water formed a broader spray cone than pentanol. The explanation is that water remains longer in droplet form and is accelerated while it is evaporated [21].
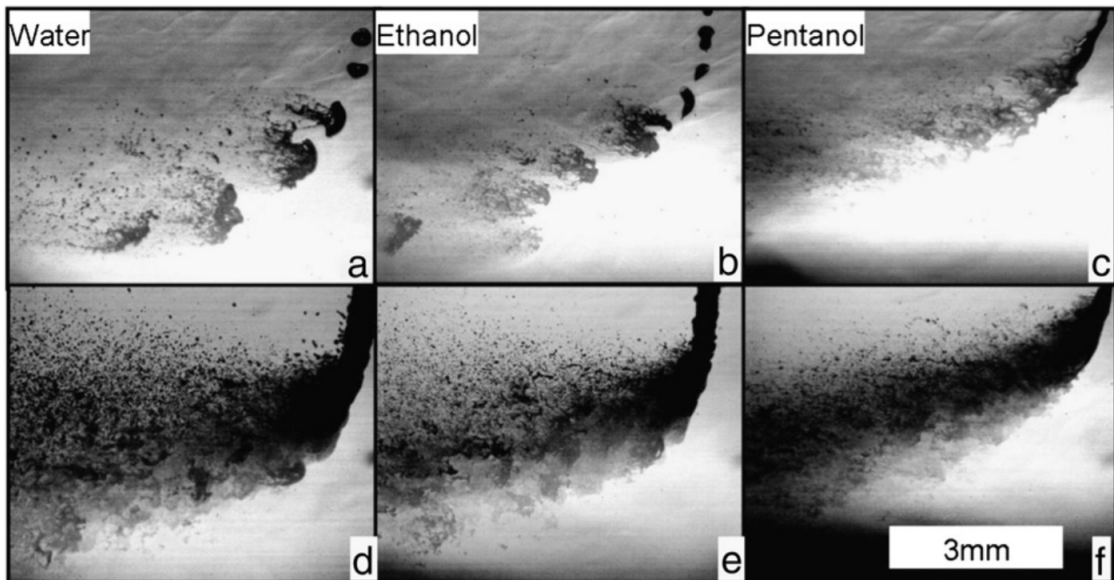
Figure 2-13: Top row — still images of different liquid injection into the same plasma (500 A, 50 slpm Ar, 20 ml/min) and bottom row — superposed image [21]

Curry et all. [22] studied the effect of changing carrier liquid from ethanol to water at 25% feedstock concentration of 8% YSZ using the 100HE plasma spray and LiquifeederHE systems (Progressive Surface, Grand Rapids, MI, USA). As shown in Figure 2-14, the one with water had more horizontal cracks and a more planar surface than the one with ethanol, which could be

justified based on poor atomization leading to larger in-flight particles, which leads to a morphology more typical in APS coatings.
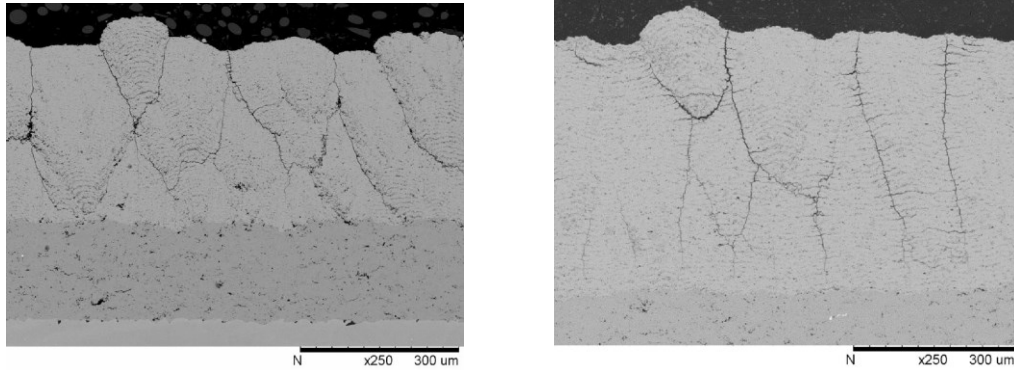
Figure 2-14: Effect of changing carrier liquid from ethanol (left) to water (right) at 25% feedstock concentration of 8% YSZ [22]

Bernard et al. [23] investigated the effect of plasma gas composition on the coating morphology of YSZ at 25% feedstock concentration using F4-VB plasma torch. Figure 2-15 shows the cross-section and surface of the coatings. Figure 2-15 (a, b) show a well-defined columnar structure formed by applying the reference gas, while figures (c, d) are the results of using a lower enthalpy gas mixture and provided broader and denser columns. The application of lower enthalpy plasma gas leads to lower temperatures in the flying particles and a lower deposition rate. Therefore, the authors concluded that due to the lower deposition of the larger non-melted particles, the share of the smaller melted particle has been increased, led to a stronger shadow effect and broader columns. Also, larger non-melted particles make the microstructure more porous and decrease the inter-columnar voids.
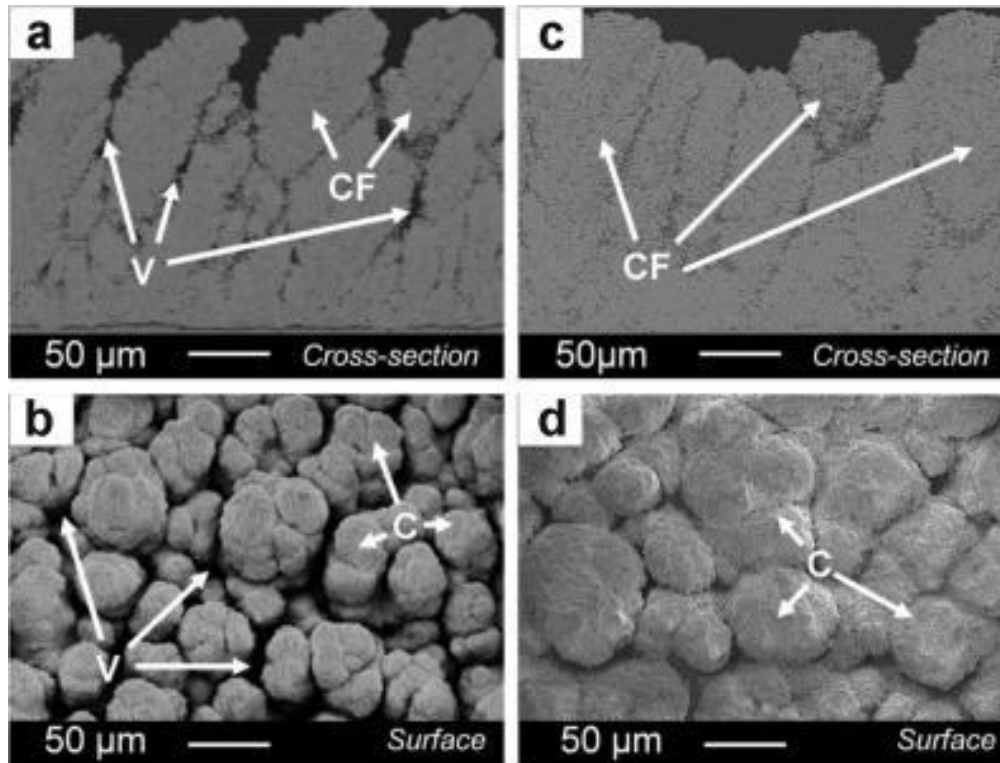
Figure 2-15: Effect of changing plasma gas from a higher enthalpy (a, b) to a lower one (c, d) on microstructure of the coating, where V, CF and C stand for inter-columnar voids, columnar features, and cauliflower shapes respectively [23]

VanEvery et al. [18] did four experiments with two different feedstock sizes of 80 nm and 15 μm of YSZ, as given in Table 1, where M and N stand for microscale and nanoscale feedstock respectively. Set up conditions are listed in Table 2.

Table 1: Experimental setup with two different feedstock sizes [18]

Suspension	Powder Conc., Wt.%	Solvent	YSZ particulate d_{50}
8M	8	Ethanol	15±6μm(volume-based)
2N	2	Ethanol	85±13nm(volume-based)
8N	8	Ethanol	85±13nm(volume-based)
11N	11	Ethanol	85±13nm(volume-based)

Table 2: Experimental setup with two different feedstock sizes [18]

Suspension	8M	2N	8N	11N
Standoff, cm	10	5	5	5
Injection pressure, MPa	29	45	45	45
Suspension flow, mL/min	42	52	52	52
Coating thickness, μm/pass	4	1	6	6

8M coating microstructure found to have a lamellar microstructure similar to APS coatings, as shown in Figure 2-16. Therefore, regardless of the induction of the SPS technique for spraying, large feedstock size was found to prevent deviation of flying particles by plasma flow and thus prevented the formation of columnar microstructure.
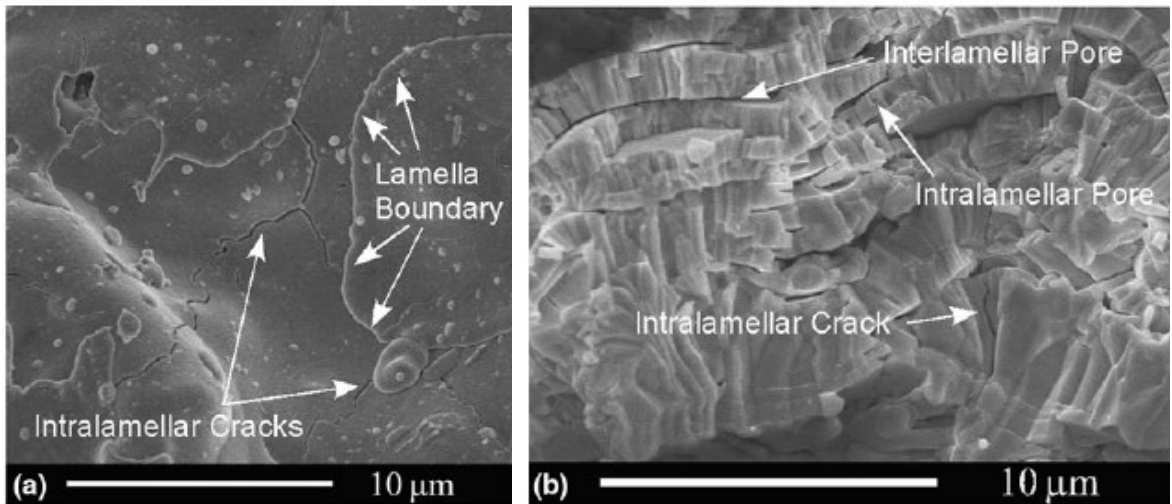
Figure 2-16: SEM images from an 8M coating showing (a) a high magnification of the top surface and (b) a fractured cross section normal to the substrate [18]

Figure 2-17 compares the microstructure of nanoparticles in different concentrations 2N, 8N, and 11N from left to right. 2N shows a very well-defined columnar microstructure while the 11N shows a vague mixed columnar format. Those results could be justified based on the fact that by increasing solution concentration, plasma heat and momentum has to be distributed among more materials, leading to poor atomization and lower temperature of the flying particles. Based on the Stokes number, larger particles impinge more perpendicularly, reduce the shadow effect, and lead to fading of columns. The same trend is also seen in images from the cross-section of those coatings. In 2N and 8N, the columnar cracks are visible through all the thickness span, while these cracks tend to get mixed in the 11N. Porosity was seen to decrease with increasing the solid loading, which was also reported by Sokołowski et al., [24]
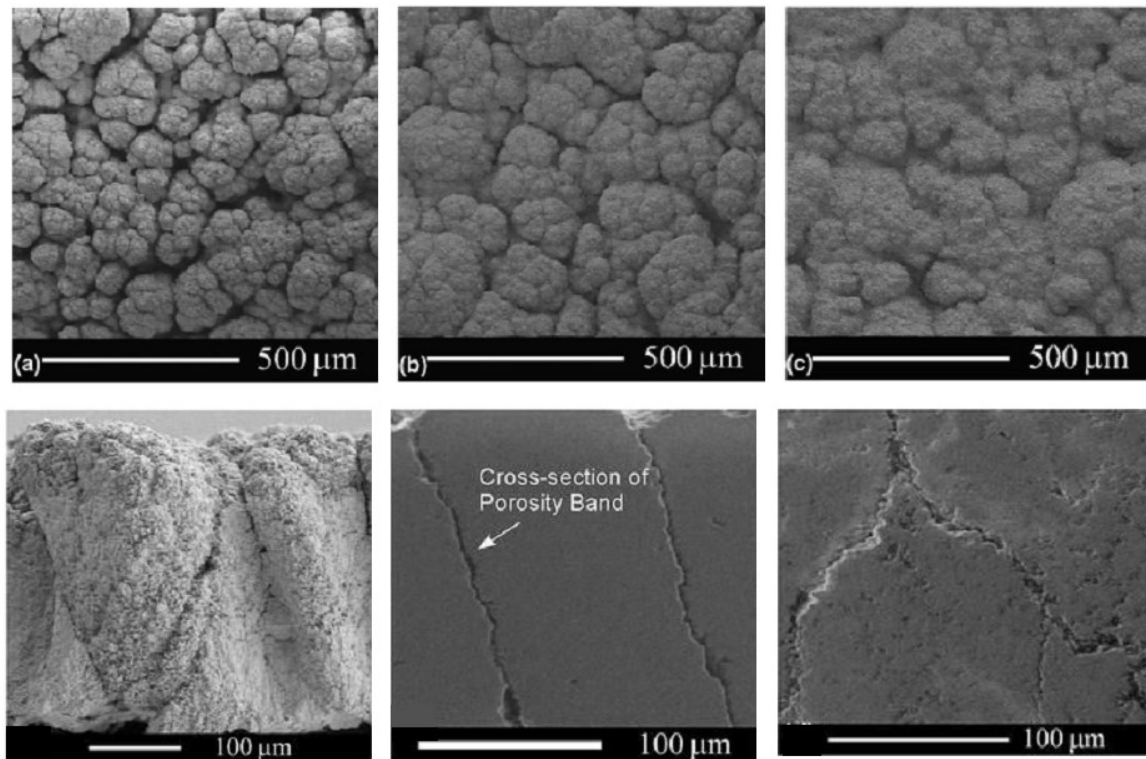
Figure 2-17: Images from top and cross section of (a) 2N, (b) 8N, and (c) 11N coatings [18]

Kromer et al. [25] investigated the effect of substrate roughness on the formation of columns in YSZ coating. They applied laser surface texturing to make cone shape asperities on the substrate. Different roughness patterns were tested to reach a uniform columnar structure from a previously optimized SPS flow. Based on their results, plateaus were found to be the critical factor inducing columnar microstructures. A sample of the textured substrate and cross-section of coating is shown in Figure 2-18. As can be seen, the build-up shows a dual characteristic. The columnar microstructure is evident on the cross-section passing peaks while those in between the mountains show a denser and more uniform aspect.
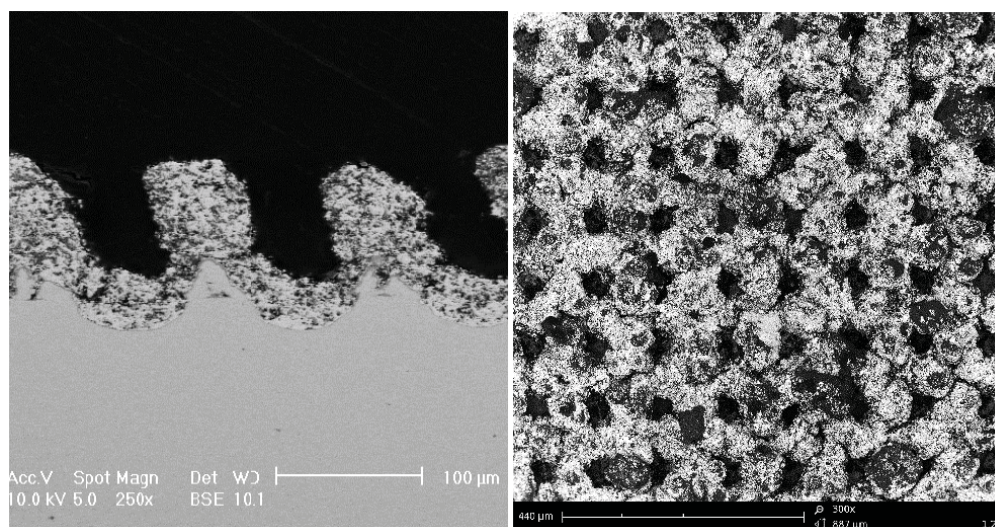
Figure 2-18: Cross-section and top surface of the optimized coating [25]

Curry et al. [26] evaluated the effects of bond coat surface roughness on the formation of columns in YSZ coatings. They applied polishing, grit-blasting, a combination of polishing and grit-blasting, and as-sprayed methods to manufacture different roughness values in the range of 1 to 12 µm, as shown in Table 3.

Table 3: Experimental coating manufacturing route and layer thickness [26]

Coating ID	Bond coat method	Surface Treatment	Surface roughness(µm)	Bond Coat Thickness(µm)	Top Coat Thickness(µm)
Plasma 1	Plasma	Polished	1-2	146±7	211±6
Plasma 2	Plasma	Polished & grit-blasted	3-4	161±9	201±11
Plasma 3	Plasma	Grit-blasted	6-8	186±12	205±9
Plasma 4	Plasma	As-sprayed	11-12	183±11	220±17
HVAF	HVAF	As-sprayed	8-9	211±8	283±10

Cross-section and the top surface of those coatings are shown in Figure 2-19. Smoother surfaces show high density of peaks and therefore lead to a high number of narrow columns, while rougher surfaces provide fewer number of asperities with a high distance from each other leading to formation of fewer and wider columns, as shown in Figure 2-19 [26].
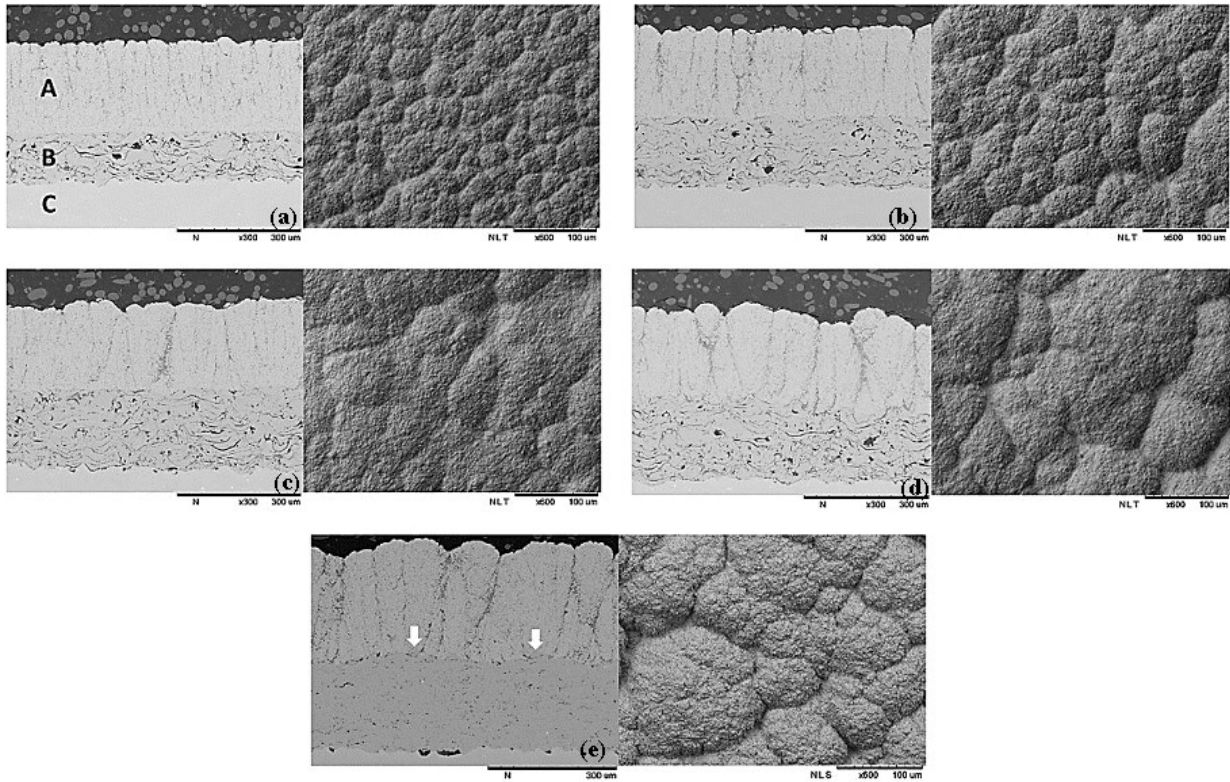
Figure 2-19:Cross-section and top surface of (a) Plasma 1, (b) Plasma 2, (c) Plasma 3, (d) Plasma 4 and (e) HVAF coatings [26]

Sokołowski et al. [27] also investigated the surface roughness effect by grid-blasting, grinding, turning and laser treatment in different solution concentration values and reported almost the same trend as Curry et al. [26] described previously. Bernard et al. [23] also stated more defined columns by increasing substrate roughness.

Curry et al. [22] tried to find out suspension properties leading to a better morphology of the spray coatings. First, they investigated the influence of three different percentages of solid loadings (33%-25%-17%) with 200 nm feedstock size suspensions of YSZ. The results confirmed what had been already reported by VanEvery et al. [18] in shifting coating from dense and vertically cracked to progressively columnar, while the deposition efficiency had an inverse trend. The cross-section achieved from the tree samples is provided in Figure 2-20.

22
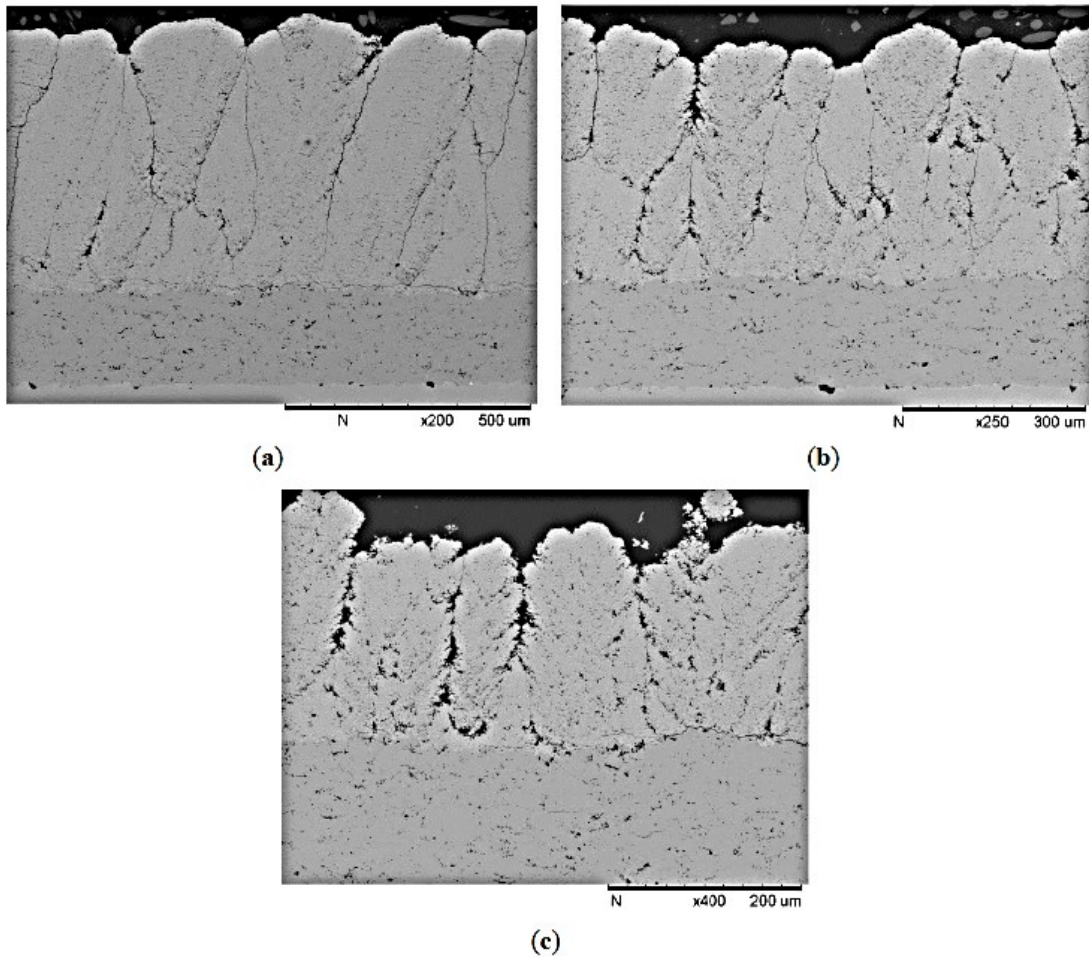
Figure 2-20: Cross section of the coating using suspension concentrations of (a) 33%, (b) 25%, and (c) 17% [22]

According to the column development theory by VanEvery et al. [18] described previously, the evolution of the column width is assumed to be directly linked to the perpendicular and lateral vectors of particle velocity close to the substrate. As described before, the lateral velocity vector comes more from smaller particles, and the normal one comes more from the larger particles. Columns could be very well-separated or very compact. Based on the shadow effect theory, expecting more compact microstructures after any change leading to higher in-flight particle diameter reinforcing perpendicular impacts, such as increasing suspension concentration or injection rate.

Bernard et al. [23] reported a more uniform and compact microstructure by increasing torch speed investigating YSZ coatings. This finding can be justified based on an equal distribution of particles, which prevents the formation of peaks or in other words weakening the shadow leading to smaller inter-columnar voids, as shown in Figure 2-21.
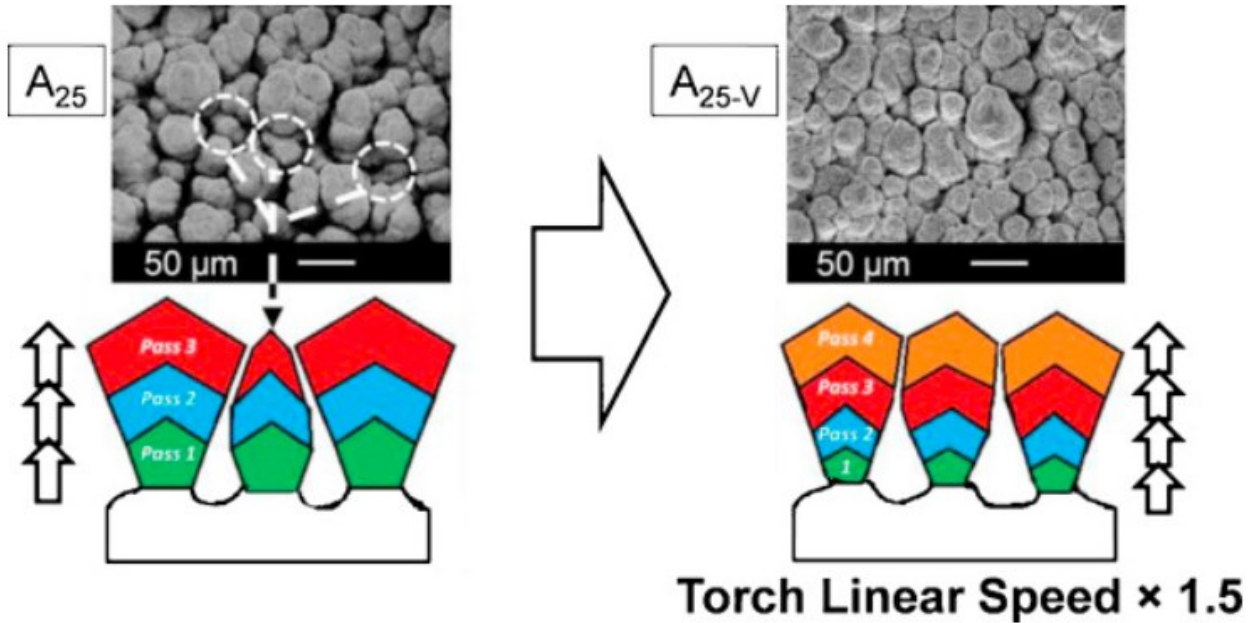
Figure 2-21: Effect of linear torch speed on microstructure of the coating [28]

Seshadri et al. [28] studied the effect of torch power on the SPS coating microstructure of YSZ keeping all other parameters constant. By increasing torch power, the plasma flow would have more thermal energy at nearly the same velocity field. Therefore, we expect to see more melted particles, which result in denser microstructures at higher powers. On the other hand, the increase in flying particle temperature leads to change in the surface tension and makes them more susceptible to atomization. It improves atomization, which, in turn, results in smaller particle and reinforces the shadow effect leading to more columnar characteristics, as shown in Figure 2-22.
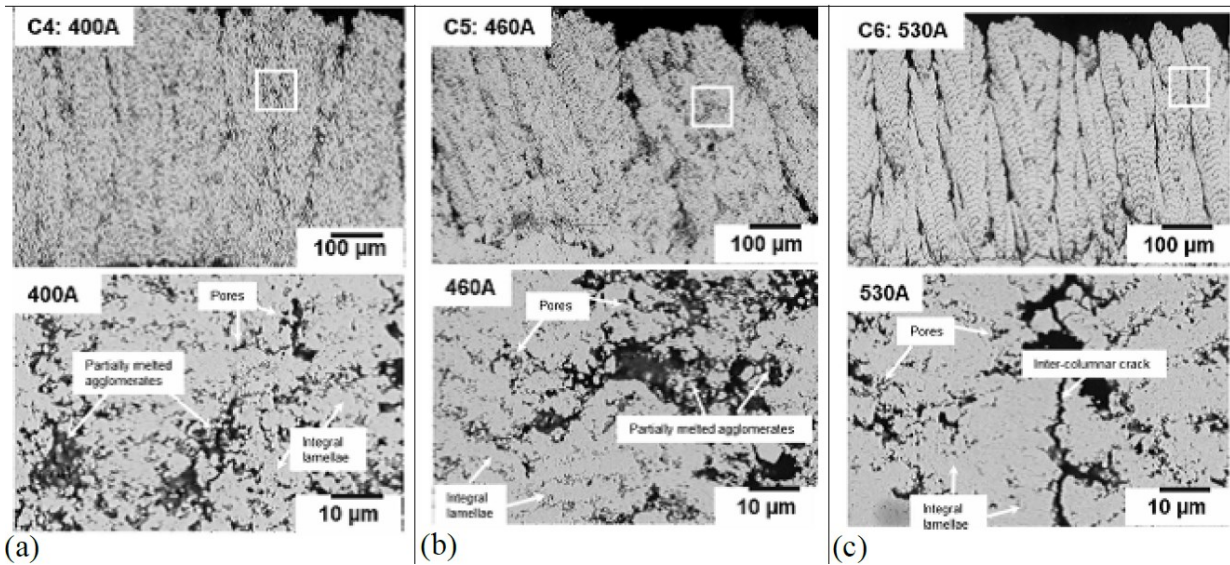
Figure 2-22: Effect of increasing torch power from low (a) to high (c) [28]

The effect of plasma flow rate on the microstructure of SPS coatings was also studied. Figure 2-23 provides the results for low, medium, and high plasma flow rates. As per these results, increasing plasma flow leads to higher velocity of plasma flow and thus better atomization, reinforcing shadow effect leading to increasing inter-columnar gap space.
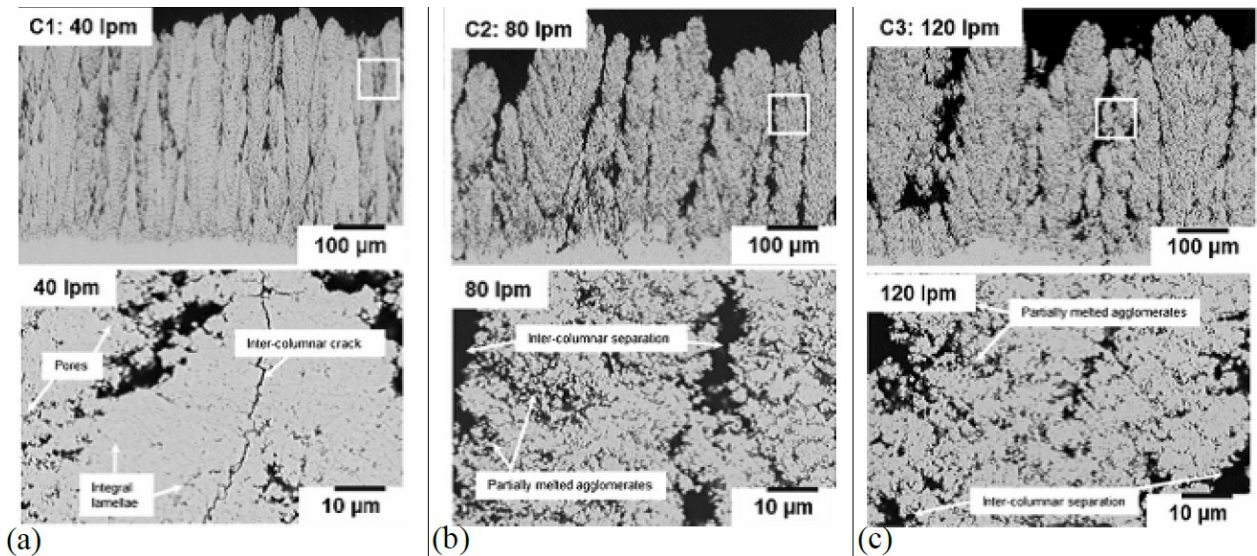
Figure 2-23: Effect of increasing plasma gas flow rate from low (left) to high (right) [28]

2.3.   Review on coating build-up simulation methodologies

As described earlier, the SPS coating microstructure depends on many factors; the effect of each one would be different from one case to another. Due to huge expenses imposed by experimental trials, scientists have always tried to find some theoretical foundations to reach at least an approximate description of the problem. Those theories would often lead to a numerical scheme applied in simulating a problem. Obviously, the numerical approaches depend on the nature of the simulated problem. For example, PVD coating build-up is a multi-scale problem, as the diffusion of the vaporized atom in the chamber is a metric scale problem, while the deposition of the adatom has to be investigated at the atomic-scale level. The first part could be tackled by applying CFD or Lattice Boltzmann theories, and the deposition of the adatom has to be investigated, considering one of the atomic interaction methodologies. Monte Carlo (MC) is one of those methods working based on the prediction of probable atomic displacements and their probability of occurrence from Molecular Dynamics (MD) or ab-initio processes.

Wang et al. [29] tried to model PVD coating build-up by applying a two-dimensional MC model. They assumed a straight line for the atomic trajectory in a gridded solution domain, which is not far from what happens in the real PVD deposition process. The trajectory angle and shooting location are chosen randomly, and the deposition location is determined based on some pre-defined assumptions, as shown in Figure 2-24. Some of the simulation results are shown in Figure 2-25, where the columnar microstructure typical in PVDs is captured. It is seen that depending on the assumed range for trajectory angles, needle or feathery like columns were predicted.
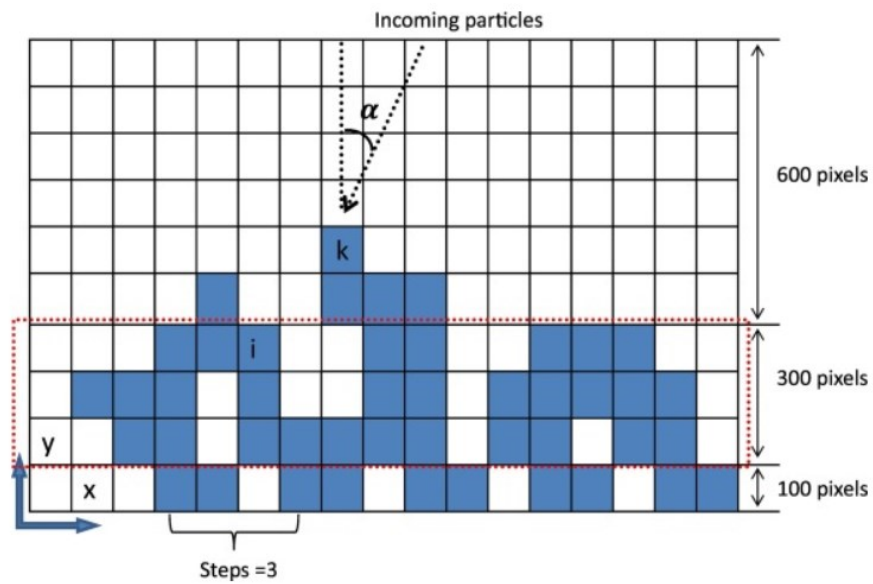
Figure 2-24: Gridded domain applied in PVD simulation by Monte Carlo method [29]
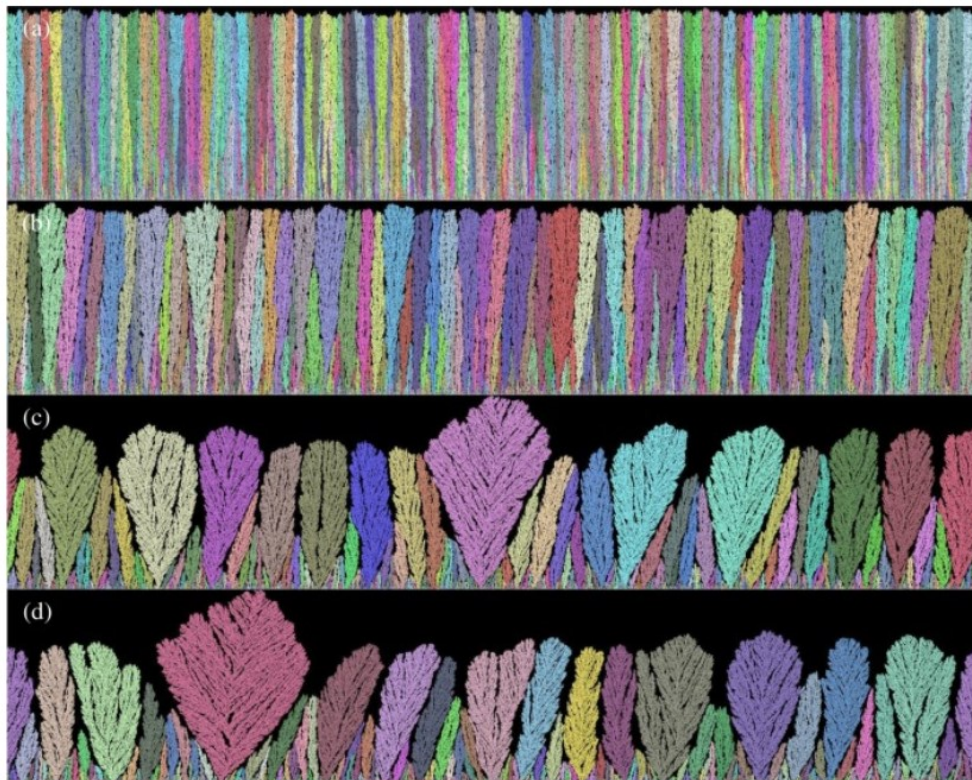
Figure 2-25: PVD coating build-up simulation results with trajectory angle limited to (a) 10º, (b) 30º, (c) 60º and (d) 90º [29]

APS coating build-up has also been extensively studied in the past 40 years. Due to the

large flying particles, the coating characteristics can be understood by investigating the physics of

a single droplet solidification. This problem consists of three phases of material, and a combination of experimental observations and CFD approaches are applied to predict the splat formation, including solidification rate, spreading ratio, and microstructure. Different theories have been followed in this regard, considering the conservation of kinetic, potential energies, and frictional forces. Depending on the experimental setup, different splat shapes may be formed, similar to what is presented in Figure 2-26.
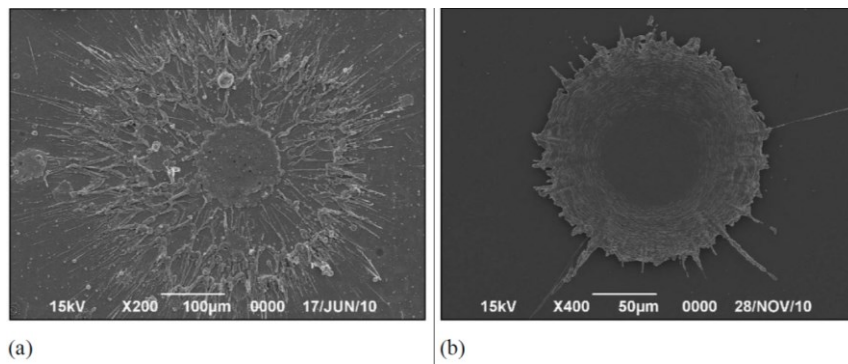
Figure 2-26: Typical splat morphologies in APS technic [30]

Cold spray coating build-up simulations consist of high kinetic large particles caused by the interaction of coating material with the high energy gas passing from the convergent-divergent nozzle. Depending on the kinetic energy of the particles, different spreading ratios are observed. The impact is mostly perpendicular and leads to the local melting and cold welding at the periphery of the impact area, shown in Figure 2-27.
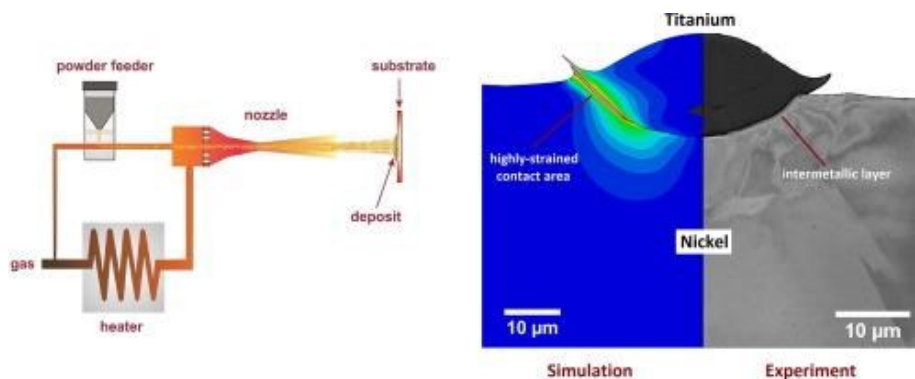
Figure 2-27: Schematic of cold spray setup and deposition simulation results [31]

2.4.   SPS coating build-up simulation

The physics of the problem in the SPS coating build-up is different from what happens in other coating techniques. Due to the relatively small size of the flying particles, the coating microstructure is not just a function of the splat morphology and is primarily controlled by the trajectory and thermal state of the flying particle close to the substrate surface. It should be mentioned that based on the Stokes number studied earlier, the trajectory of the flying particles is a function of particle size and cannot be randomly chosen by a Monte Carlo methodology, as applied in other thermal spray techniques [32] and the PVD coating build-up simulations. Besides, due to the small size of the particles in SPS, there is negligible splashing and the solidification is nearly instant. Compared to the case of cold spray technic, the kinetics of the particles is not enough to follow the same mechanism of deposition. Therefore, SPS coating build-up is a unique process which has to be investigated from a different perspective.

To the best knowledge of the author, the only published SPS coating build-up modeling is the one from Ghafouri Azar [2]. In this study, the particle characteristics were computed according to the work of Pourang et al. [3]. The particle characteristics 100 μm from the substrate surface are used to build a database from which the coating buildup will be simulated. Figure 2-28 shows particles normal velocity impacting a flat and a curved substrate.

The coating buildup model made use of a uniform gridded computational domain, each grid being either empty or filled if a particle landed at this specific location. Therefore, all the particles were assumed to have the same shape and size conformal to the grid, and the flattening process was not taken into account. By making some assumptions, the deposition location of each particle was computed, leading to the formation of a 3D coating. The current study will build on

some concepts taken by Ghafouri Azar [2], and therefore this model will be described in detail in the following.
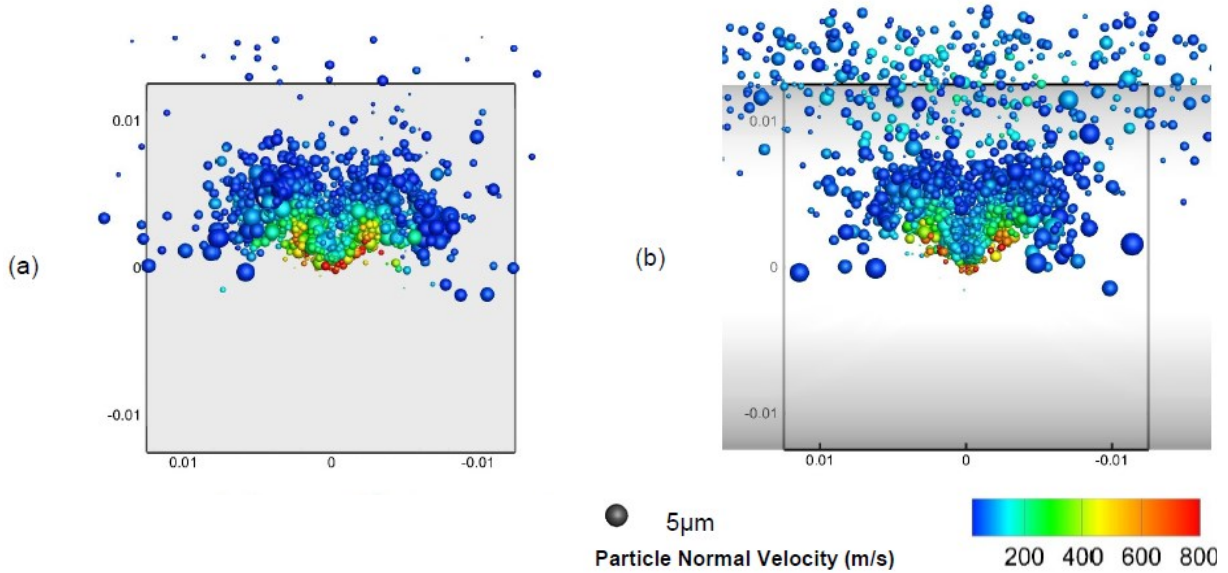
Figure 2-28: SPS numerical simulation results showing the distribution of particles and their normal velocity before impacting a (a) flat and (b) curved substrate [3]

Ghafouri Azar [2] introduced a 3D model in the simulation of SPS coating build-up on substrates with different geometries. He developed a tool in MATLAB, assuming that:

1. The coating particles follow a straight trajectory from 100 µm above the substrate to the substrate surface

2. Flattening of the particle on the substrate has a negligible effect on the final coating microstructure

3. A gridded domain could be applied to form the coating build-up

4. Coating particles are considered as cubes of 1 µm^3

5. Substrate roughness are modeled as cone shapes

The first assumption came from the fact that the particle distribution data from Pourang et al. [3] was provided at 100 µm distance from the substrate. Due to a lack of data regarding the

30

particle trajectory before impingement, Ghafouri Azar [2] considered the particles to have fixed velocity vectors and thus linear trace lines.

Regarding the fourth assumption, considering the gridded domain of solution, he had to assume all flying particles to have the same size specified in the grid, 1 μm dimensions. He also made assumptions regarding the deposition location of the particle in the gridded domain. Depending on the trajectory angle and direction of the particle, it could be stored in one of the 17 possible cells around the impacted particle on the coating surface, as shown in Figure 2-29.
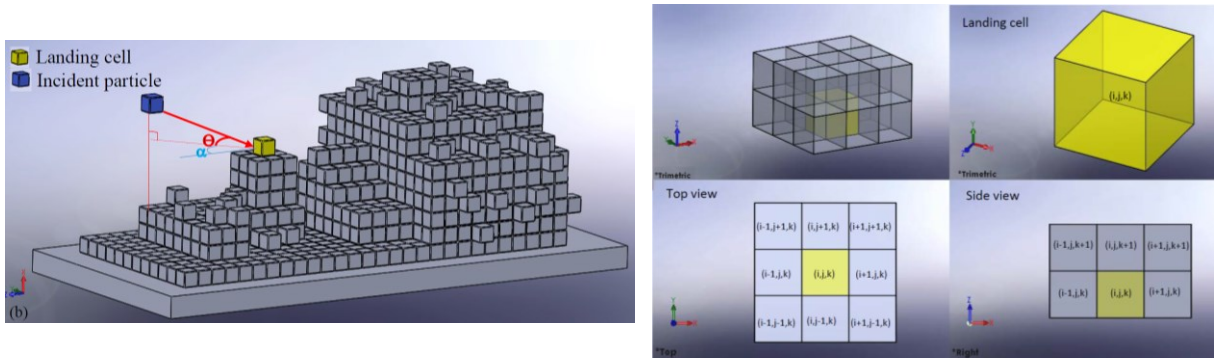
Figure 2-29: Schematic of SPS coating build-up model by Ghafouri Azar [2]

The cartesian coordinate system was applied in that study. The z-axis considered to be perpendicular to the substrate, x-axis as the torch sweeping direction, y-axis in raster interspace direction, and the origin is chosen to be on the edge of the modeled area. Figure 2-30 shows a schematic of the problem.
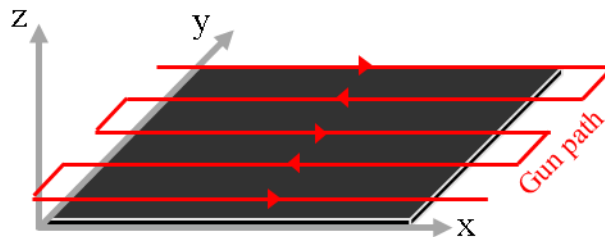
Figure 2-30: Torch sweeping path in Ghafouri Azar [2] model

The coating particle distribution, taken from Pourang et al. [3] results at 100 μm distance in front of the substrate, was introduced to the model in the form of parcels, as in Table 4:

Table 4: In-flight particles characteristics from CFD

	x_p	y_p	z_p	v_{xp}	v_{yp}	v_{zp}	d_p	T_p	N_p
Parcel 1	-	-	-	-	-	-	-	-	-
Parcel 2	-	-	-	-	-	-	-	-	-
…	-	-	-	-	-	-	-	-	-

Where

- x_p, y_p, and z_p are the coordinates as defined in section relative to the torch axis

- v_{xp}, v_{yp}, and v_{zp} provide the velocity vectors in different directions

- d_p, T_p, and N_p are the diameter, temperature and number of particles in a specific parcel, respectively

Ghafouri Azar's computation showed to be very time-consuming. Therefore, he had to limit the solution domain to save some computational cost. Consequently, he considered a 200x200 μm² square for investigating the coating build-up microstructure referred to as "interested area". However, to avoid to edge effect, he had to consider a larger modeling square, referred to as "Modeled Area", of a 600 x 600 μm² side. Figure 2-31 shows a schematic of the computational area.
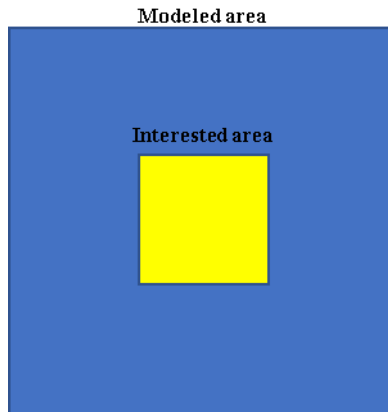
Figure 2-31: Schematic of "interested: and "modeled" areas in Ghafouri Azar [2] model

The transversal torch speed was set to 1 m/s, while the travel line was broken into 1 μm steps to consider coating build-up with 1 μs intervals.

We know that in the atomization and spraying problems, randomness comes naturally as a part of these processes. Computational methods involved in simulating the process also take into account this randomness, however due to limitations regarding computational costs, the results cannot cover all the probabilities. For example, in Pourang et al. [3] model, the dataset particles injected from a specific torch position cannot cover every spot on the substrate. To tackle this problem, Ghafouri Azar [2] added a randomness factor to the exact landing location of the particles.

For a specific location of the plasma torch, the solution steps are as following:

1) The landing particles on the Modeled Area were found

2) 10 particles were chosen randomly between the landing particles

3) After adding randomness, the impact location of the particles of step 2 were found

4) Torch moved to the new location on the travel line at 1-μm distance from the current location.

Figure 2-32 shows the results of the coating build-up for the torch sweeping a full raster. As can be seen, the coating has not developed enough to enable the analysis process. In fact, due to the high computational cost burden by the applied method, developing those results took more than six months.
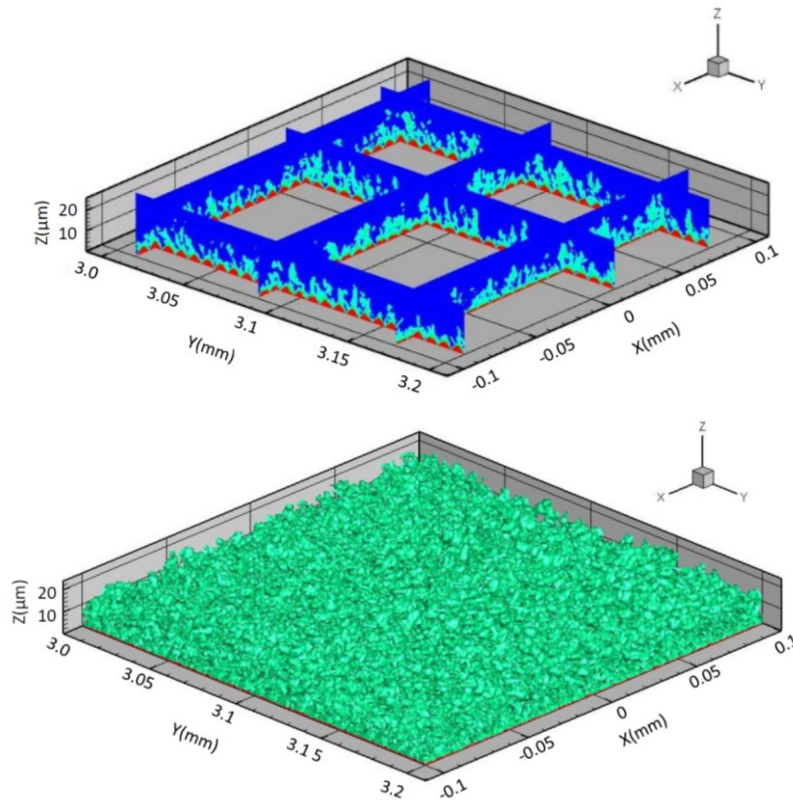
Figure 2-32: SPS coating build-up by Ghafouri Azar [2] model

Regarding the limitations of the mentioned method, any new algorithm should be fast enough to enable the investigation of different parameters on the coating microstructure. In response to this demand, a new meshless methodology was developed. In this new algorithm, the actual particle size can be taken into account, there is no need for any assumptions regarding the deposition location of particles, and the continuity could be conserved more accurately. This is the object of this thesis.

Chapter 3.   Computational Methodology

In this chapter, the developed coating build-up simulation method is described including the considered assumptions and the applied equations.

There are some key words frequently used in this chapter as defined below:

Modelled area	: The 600 in 600 µm area in which the coating build-up is modelled
Interested area	: The 200 in 200 µm area in which the coating microstructure will be investigated
Already deposited particles	: The particles deposited on the substrate as a part of coating
Landing particles	: The particles which land on the "modelled" area
Shot particles	: The particle which its landing position will be calculated as a part of the simulation process
Flying particles	: The particle at 100 µm distance relative to the coating surface
Probable landing particles	: The flying particles which will land on the "modelled" area before applying the randomization
Probable impact particles	: The already deposited particles which the investigated flying particle would impact to

3.1. Assumptions

The following assumptions were made

1) The   coating particles follow a straight trajectory all the way from 100 µm above to the substrate surface, as shown in Figure 3-1. The direction of flight is based on the velocity vectors at the starting position.
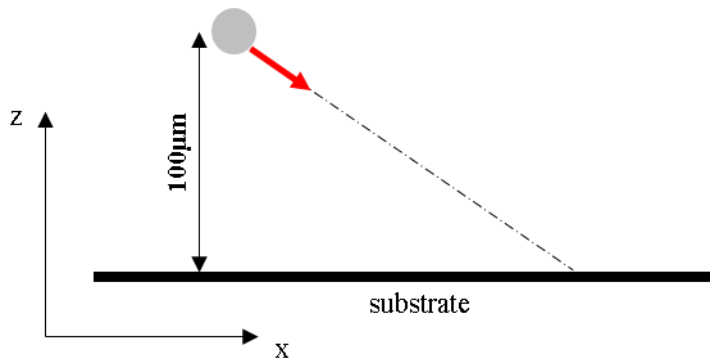
Figure 3-1: Schematic of a flying particle trajectory

2) As the coating grows, the roughness of the coating surface changes for the initial roughness of the substrate. Therefore, the trajectory of the flying particles can change. It is assumed that the change in particle trajectory is negligible, and thus the same set of data will be applicable through all the simulation process from the beginning of the deposition to its end. As the coating grows, the height of the flying particles will also be modified to keep the relative 100 µm distance from the coating surface.

3) Particles deposit at the impact location, and the rebounding, splashing is considered to be negligible.

3.2. Inputs

The required settings and input data necessary for the starting of the simulations are discussed in this section.

1.1.1. Substrate geometry

Substrate asperities are made by piling uniform-diameter spheres at a size specified by the user. By using this technique, any substrate roughness can be simulated. For example, it can be built from the cloud of points from a confocal microscope image of a real substrate surface. In this study, asperities are modeled as pyramids, as shown in Figure 3-2.

Figure 3-2: Substrate geometry simulated by cone shaped asperities

1.1.2. CFD data

The particle distribution at 100 μm above the substrate level is extracted from CFD simulations by Pourang et al. [3], simulating the 3MB Oerlikon-Metco torch with a 20-mm long anode and a 6-mm diameter exit nozzle, and a 2.5 x 2.5 cm^2 substrate, as shown in Figure 3-3.
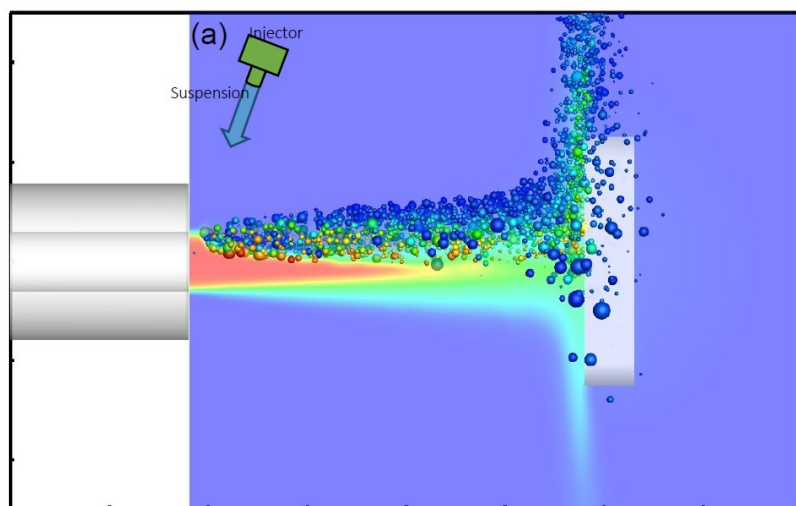
Figure 3-3:   Coating particles from 3MB torch simulation [3]

KHRT breakup model was applied in the CFD simulations, which is a stochastic methodology considering both Rayleigh-Taylor instabilities; coming from the acceleration of the newly formed droplets, and Kelvin-Helmholtz waves; induced from aerodynamic forces instabilities. Torch setup and material properties are shown in Table 5 and Table 6. In this setup injection rate set to 0.5g/s at a 10% feedstock concentration and 14-degree backward injection angle.

Table 5: Computational settings applied by Pourang et al. [3] simulating 3MB torch

Arc Current(A)	Arc Voltage(V)	$Ar - H_2$ mass flow rate (gr/s)
500	65	1.48 (10% $volume\ fraction$)

Table 6: Material properties incorporated in modeling 3MB torch by Pourang et al. [3]

	Units	Molten zirconia	Ethanol
Density	kg/m^3	5680	789
Specific heat	$J/kg.K$	1387	2470
Surface tension	N/m	1.5	0.0223
Melting point	K	2988	…
Boiling point	K	5273	351
Viscosity	m^2/s	6.5e-6	1.2e-03
Melting latent heat	J/kg	707e3	…
Boiling latent heat	J/kg	9e6	855237

Figure 3-4 shows the trajectory of the particle distribution from 100 μm above (arrowhead) to the substrate level (arrow end). The red point corresponds to the torch axis. As can be seen, the majority of the particles are located above the torch axis and therefore the injected suspension has not diffused thoroughly inside the plasma core. It is important to note that in Pourang's work, the plasma jet is considered constant neglecting the influence of the plasma fluctuations.
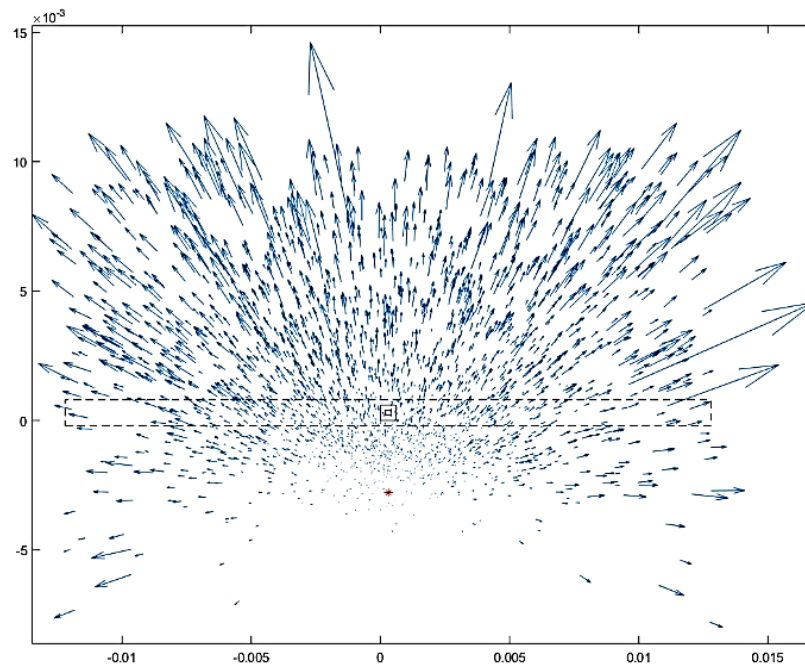
Figure 3-4:Flying particle distribution and trajectories at 100 µm above the substrate level

3.3. Coating build-up simulation

Two different simulation strategies are introduced as "frozen" and "flattened" models. The frozen model assumes a solid deposition of the flying particle at the impact location, that is to say, the spherical shape of the particle stays the same after landing. In contrast, the flattened model takes into account the flattening of the particle. The same computational approach has been followed in the development of both models, except the splat formation. In the following section, the steps in setting up the coating simulation common between both models will be explained and the calculations regarding the geometry of the deposited particle will be addressed in the following section.

3.3.1. Setting up the simulation

In this section, the procedure of setting-up a coating simulation is discussed by explaining variables and concepts considered in developing the current tool. As discussed earlier, two different models regarding the splat geometry will be investigated. It should be mentioned that setting up the problem is the same for both models and the only difference will be

3.3.1.1.   Setting up the problem

1) The particle distribution from the CFD results is the database used by the coating build-up model providing the following information for every single set of parcels, as shown in Table 7. It should be mentioned that a parcel introduces a group of particles with the same characteristics.

Table 7: Flying particles characteristics at 100 μm above the substrate as calculated from the CFD results

	x_p	y_p	z_p	v_{xp}	v_{yp}	v_{zp}	d_p	T_p	N_p
Parcel 1	-	-	-	-	-	-	-	-	-
Parcel 2	-	-	-	-	-	-	-	-	-
...	-	-	-	-	-	-	-	-	-

Where

- x_p, y_p, and z_p are the coordinates as defined in section 2.4. relative to the torch axis

- v_{xp}, v_{yp}, and v_{zp} provide the velocity vectors in different directions

- d_p, T_p, and N_p are diameter, temperature and number of particles of the parcel respectively

2) Defining substrate geometry

40

Substrate geometry is defined by providing the shape of the pyramids, interspace, and, finally, the embedded sphere size, as shown in Figure 3-2.

3) Defining torch sweeping pattern

4) Defining the dimensions and location of simulation area as explained previously in section 2.4.

5) Calculating the "gap space"

In this step, the distance of each parcel of the dataset from the nearest parcel in its neighborhood is calculated. Then the mass average of those distances is calculated and divided into two, to represent the average distance of two parcels in the database, referred to as "gap space" shown by L_{ave}. The random distance of a specific particle in the x and y directions would be calculated by multiplying a random number, between zero less than one, in L_{ave}.

$$x_r = L_{ave} * rand$$
$$y_r = L_{ave} * rand$$

3.3.1.2.   Coating build-up simulation steps

1) Finding the "database representative time"

From the problem setup, we know the injection rate, and also the concentration of the solution, which gives us the feedstock injection rate per second. From the other side, we can calculate the mass of the dataset. Dividing those two values provides us with the interval represented by the CFD simulation, referred to as "database representative time."

2) Finding the injected coating mass in 1 μs

The total mass of the dataset is calculated and divided into database representative time to gives us the mass of the feedstock injected in 1μs, where ρ_p is the particle density and N_p is the number of particles in a parcel.

$$M_{inj} = \sum N_p m_p / \Delta t_{rep}$$

$$m_p = \frac{\pi}{6} d_p{}^3 \rho_p$$

3) Finding probable landing particles:

Based on the velocity vectors of the flying particles, their landing location at the substrate level could be calculated

$$\Delta t_{land} = \frac{100 \ (\mu m)}{v_{zp}}$$

$$X_{land} = x_p + v_{xp} \Delta t_{land}$$

$$Y_{land} = y_p + v_{yp} \Delta t_{land}$$

Where x_p and y_p are the location of the particles at 100 μm above the substrate level. All the particles in the "modeled area" are then listed as the probable landing particles.

4) The mass-based average diameter of the enlisted parcels is as follow:

$$\bar{d} = \frac{\sum d_p N_p m_p}{\sum N_p m_p}$$

giving

$$\bar{m} = \frac{\pi}{6} \bar{d}^3 \rho$$

5) The number of injected particles comes from dividing numbers from steps 2 and 4.

$$N_{inj} = \frac{M_{inj}}{\bar{m}}$$

Finally, a random function based on parcels mass is applied to choose among the probable landing particles.

3.3.1.3.   *Randomizing injected particles location*

Random values limited to gap space value as defined previously are added to x_p and y_p

$$x_p = x_p + x_r$$

$$y_p = y_p + y_r$$

3.3.1.4.   *Finding impingement location of the considered landing particles*

In this step, deposited particles are stored in a matrix, including their location and dimension. The flying particle would impact one of those already deposited particles, or land on the substrate. The impinging location could be easily found based on the particle location, trajectory, and diameter as following.

- First, all the already deposited particles which are located at a range of distance, less than the average of their and the flying particle diameters, from flying particle trajectory are listed, which are called the probable impact particles, as shown in Figure 3-5.

$$D_s \leq (d_p + d_s)/2$$

D_s :   Already deposited particle distance from flying-particle trajectory line

d_p: Flying particle diameter

d_s: Substrate deposited particle diameter
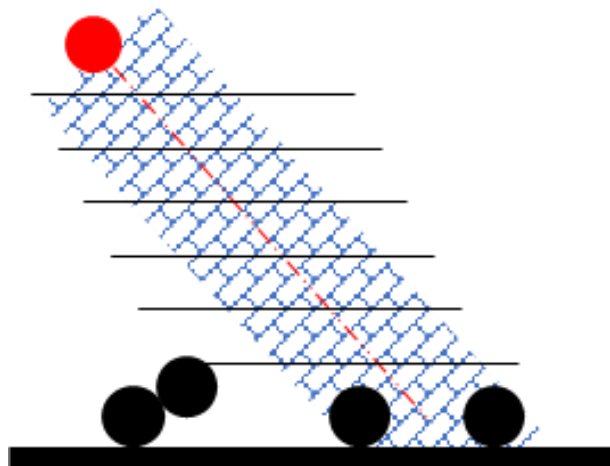
Figure 3-5: Schematic of coating particle trajectory and probable impact particles

- In this step, the impact interval for the enlisted probable impact particles is calculated to find the impacting particle and the landing location accordingly.

- In this step depending on the chosen frozen or flattened model, the geometry of the splat should be calculated. In the case of the frozen model, the solution of the particle deposition finalizes after finding the impact location, while in the flattened model a specific procedure has to be followed as discussed in the next section.

This procedure will be followed for all the shooting particles.

3.3.1.5. *Moving the torch and database*

Along the torch pattern: The torch and the flying particles are transformed along the torch travel line by 1 µm as the torch speed is 1 m/s and the simulation intervals are 1 µs.

Perpendicular to the substrate: The maximum height of the coating is calculated after the deposition of every single particle. After every 5 µm increase in the coating thickness, the torch height is updated to keep the 100 µm relative distance to the average height of the coating surface.

3.3.2. Frozen and flattened models

As discussed earlier, splat geometry will be investigated considering two different theories, as is discussed in this section.

3.3.2.1. Frozen model

In SPS, particles of sizes ranging from a few hundred nanometers to a few micrometers are deposited. These small particles, which also have a significant temperature difference with the substrate, get frozen fast enough to prevent substantial particle deformation. From another point of view, small particles follow the plasma streamlines, and therefore, the perpendicular velocity vector would be low enough to neglect the flattening. These two facts justify the solid impact

assumption considered in the frozen model. Setup conditions such as high injection rate, low torch power, and high stand-off distance could be the candidates for applying the frozen model.

In this method, the calculations regarding the geometry of the deposited particle finalize after finding the impact location, as there would be no change in the original shape of the particle after deposition.

3.3.2.2. Flattened model

The droplet flattening process has been widely investigated during the last four decades, both numerically and empirically, though the majority of cases are with particles in the range of twenty to a few hundred micrometers. The dominant factors controlling the final shape of a flattened particle are the surface tension (capillary) and viscosity as the limiters and kinetic energy as the driver. In most cases, the droplet temperature is higher than its melting point, and it begins to solidify after impingement. Solidification might be seen as a limiting factor regarding the flattening ratio. However, studies show splat solidification ends after the flattening process. Splashing, surface roughness, and splat-substrate interaction also affect the splat geometry and add to the complexity of the problem. Splat shape could also be a function of the impingement angle as observed by investigations of the SPS splats on the glass Figure 3-6.
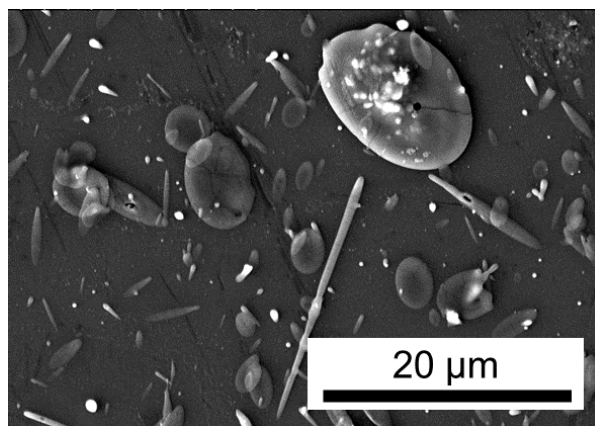
Figure 3-6: SPS splat on glass [courtesy of N. Sharifi-Concordia university]

Despite the complexity of the problem, regarding the relatively small characteristic length of the particles in SPS, most of those influencing parameters, such as splash and temperature difference between particle and substrate, can be easily neglected, which gives a chance to benefit a relatively simple flattening model. It should be mentioned that due to the small size of the particles in SPS, the size of splats is negligible compared to the size of columns, and therefore the splat geometry is believed not to influence the final coating microstructure. This belief will be investigated by comparing the coating microstructures of two different deposition models, called frozen and flattened models, regarding the geometry of the splat.

In the flattened model, the splat shape is modeled by applying a group of smaller spheres with a diameter equal to the assumed splat thickness, as shown in Figure 3-7. It can be seen that the splat is assumed to form a kite shape with the elongated axis along the direction of the particle just before its impact. Depending on the diameter of the small particles, the kite area will be adjusted to conserve the same volume as the original sphere. It should be mentioned that following this methodology leaves free spaces between spheres, which provides room for particles to diffuse through, as shown in Figure 3-8. To tackle this problem, mediate spheres were incorporated to fill the space and minimize errors.
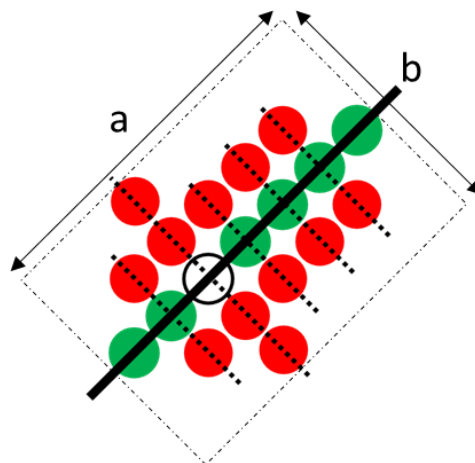
Figure 3-7: Forming the original splat geometry by smaller spheres
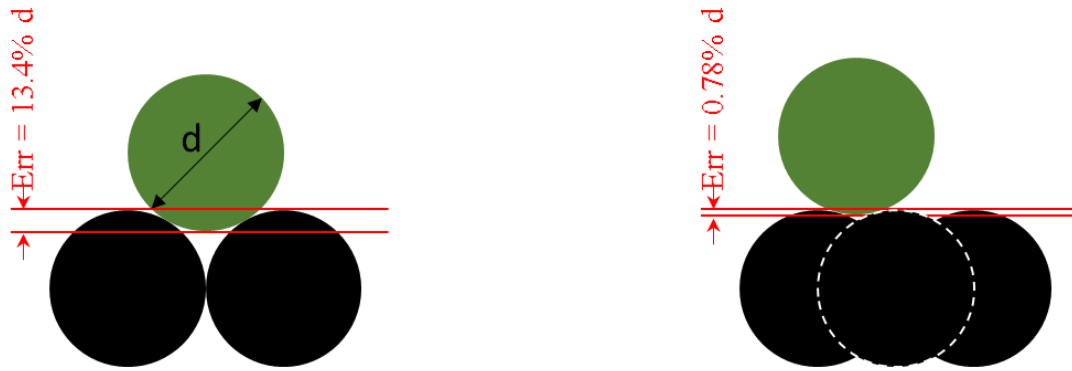
Figure 3-8: Error from the interspace between the constituent small spheres

Different ideas were investigated regarding the connection of smaller constituent particles, as shown in Figure 3-9. In "Raining" model the integrity of particle is not considered and also the "Carpet" model tends to overpredict the porosity of the coating. While the "adaptive" model addresses both of those issues and therefore provides a better representation of the splat geometry. However, keeping the integration of the small constituent particles in adaptive model necessitates unaffordable computational cost. To tackle this problem, integrity is preserved just in the longitudinal direction, as was shown in. It should be mentioned that the splat has the maximum width at the impact location and gets narrower as it develops in the longitudinal direction which justifies the kite shape of the splat.
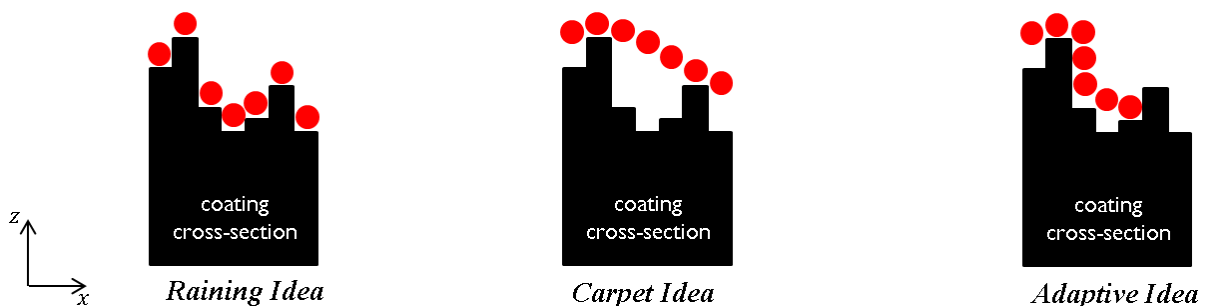
Figure 3-9: Different splat deposition ideas followed in the flattened model

The dimensions of the kite are calculated as below:

- From the continuity, the volume of the splat must be equal to the original particle.

  By equalizing the kite volume and the original sphere we get

47

$$ab/2(FR * d_p) = 4/3\pi\left(\frac{d_p{}^3}{8}\right)$$

Or

$$ab = \pi\frac{d_p{}^2}{3FR}$$

Where D, a, b, and FR represent the particle diameter, longer and shorter diameter of splat, and flattening ratio respectively. It should be considered that the flattening ratio applied in the flattened model results are considered to be three unless otherwise noted.

- on the other hand, we know that for perpendicular impact, a and b are equal, and in this condition b has its maximum value.

$$b_{max} = \sqrt{\pi\frac{d_p{}^2}{3FR}}$$

To have the variation of b relative to the impact angle, different correlations could be considered. For now, we assume that

$$b = b_{max} \sin\sin\gamma$$

Where γ represents the impact angle relative to the substrate level. Then a can be calculated accordingly from the continuity equation.

The splat geometry is then found by following these steps:

1. Impact location is detected based on the impact point of the original-flying particle and coating surface, and a constituent particle is placed at the impact location

2. Particles in both longitudinal directions are placed one by one in a way to be tangent to the adjacent particle in the master direction and placed on top of the underlying sphere.

3. Particles in branches of each master particle called "slave" direction are placed in a way to be tangent to the last particle in the Slave direction and be placed on top of the underlying sphere.

A view of the two droplets impinged one on top of the other is shown in Figure 3-10.
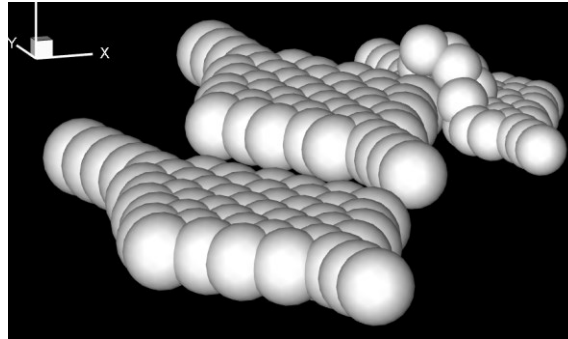
Figure 3-10: View of piling of particles in flattened model

The flattened model still is expected to overestimate porosity due to overestimating inter-space between different deposited particles, as shown in Figure 3-11.

Figure 3-11: unfilled space (in brown) between two flattened particles in the flattened model

3.4. Simulation set-up and results

The results of the coating build-up modeling provided in the next chapter are based on the input data from Pourang et al. [3] study. The results will be reported typically by showing a slice of the coating with a thickness of 10 μm. This cross-section view could be parallel or perpendicular to the torch movement along the x axis. Figure 3-12 shows a perspective of a coating cross-section (left) and the way it gets represented as a result with a cross-section perpendicular to the torch movement (right). Red spheres are used to show the initial roughness asperities of the substrate

and white ones show the deposited particles. Cross-sections are chosen to be centered on the roughness peaks and close to the middle of the interested area.
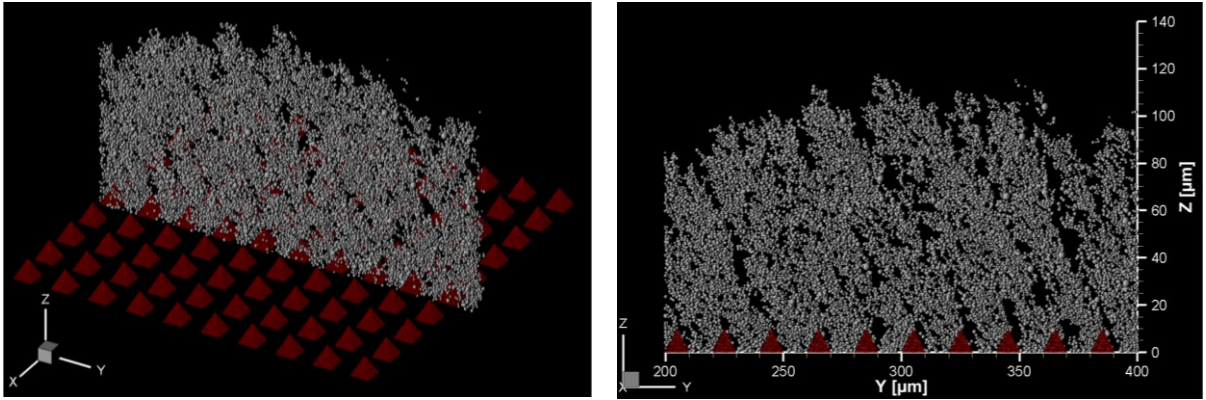
Figure 3-12: perspective to a slice of coating (left) and its result preview (right)

Three different patterns of torch movement were studied in this study called perpendicular-linear, linear and full-raster, as respectively shown with red, green and black lines in Figure 3-13. In the linear and perpendicular-linear cases, the torch sweeps a line at three millimeters below, and middle of the modeled area, respectively. It has to be mentioned that the landing particles which are closer to the torch axis, provide particles with a more perpendicular trajectory and the perpendicular-linear configuration is named regarding this reality. In the case of the full raster, the torch sweeps lines parallel to the x-axis with a 3 mm interspace in between.
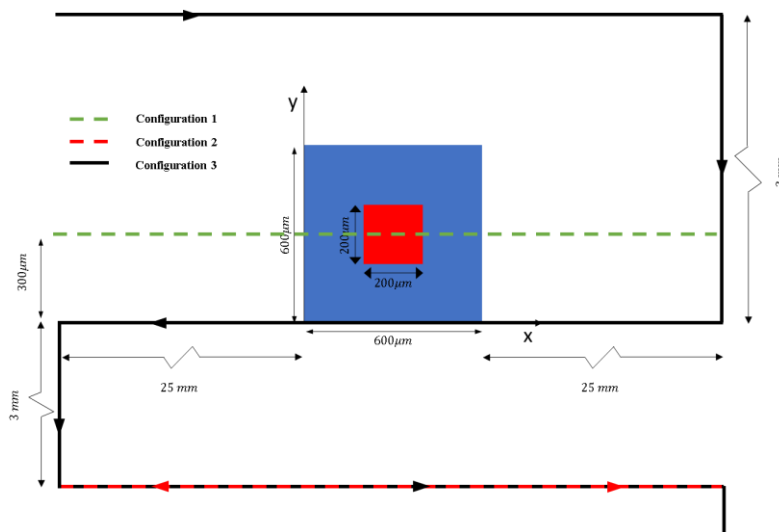
Figure 3-13: Torch pattern relative to the substrate, green and red lines (linear), and black line (full raster)

Chapter 4.   Results and Discussions

In this chapter, the simulation results from the developed tool are investigated. Some key parameters affecting the coating build-up are studied and compared to the theories and experimental investigations reviewed in the last chapters. To help a better understanding, the simulation results are divided into two sections based on the torch sweeping configuration, as linear-raster and full-raster explained previously. In the first section, frozen and flattened models are compared, followed by studies on the effect of substrate geometry, flattening ratio, and particle trajectory. In the second section, the results are provided just for the flattened model where the build-up history, substrate geometry and torch speed are studied. It should be mentioned that the frozen and flattened models both involve the same computational methodology with a difference in flattening ratio. In fact, the frozen model represents the extreme case of solid deposition, where the flattened model assumes the formation of splats with FR equal to three for all the depositing particles. Reality involves a range of FRs depending on the Reynolds and Weber number of the particles which can be introduced into the code based on some correlations, in the future.

4.1. Results for the linear raster

4.1.1. Coating build-up on smooth substrate

Figure 4-1 presents a cross-section of the coating build-up results for a similar simulation of coating on a smooth substrate by the frozen and flattened. As can be seen both cases show a

dense layer adjacent to the substrate, and after a transition phase, columns start to grow. This observation could be justified based on the fact that at the beginning of the process, due to the absence of asperities, there is no shadow effect, leading to an unstructured and dense morphology. After a while, some peaks would be created randomly due to the particle deposition, which acts efficiently in piling the flying particles making them grow faster and make the column bases. It should be mentioned that the growth of columns corresponds to the direction of flying particles in the y-z plane, as expected.
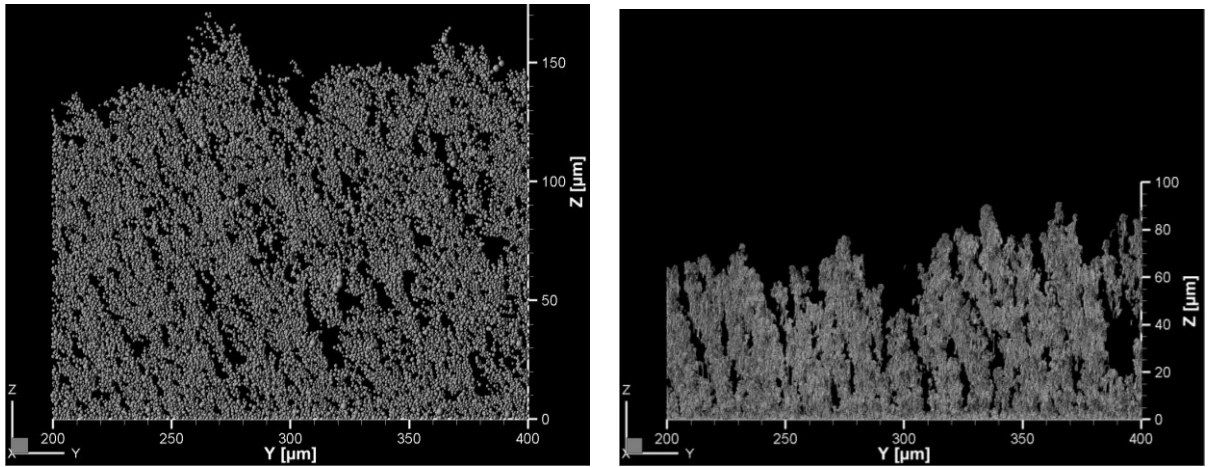
Figure 4-1: Simulation results for linear sweeping and smooth substrate by frozen (left) and flattened (right) models for 10 paths

The flattened model predicts a denser microstructure and lower coating growth rate, for exactly the same experiment. The reason would be the stronger shadow effect made by the deposition of original flying particles compared to the smaller flattened particles. On the other hand, the column growth angle is more perpendicular in the flattened case. This can be justified according to Figure 4-1, where the dash lines show the column growth direction. In the flattened model due to the spreading of the particles, local growth of the peak is damped and distributed, giving the flattened particle a chance to pass to the shadow side, in turn leading to a more perpendicular growth of columns. The green lines are drawn in parallel with the direction of flying particles and tangent to the highest deposited particle to show an approximation of the shadow

52

length made by the peaks with similar coating heights. As can be seen, the flattened case makes a longer shadow, and thus a more defined columnar inter-space. It could be said that the longer shadow in the flattened model keeps the columns separated and leads to overestimation of intercolumnar space compared to the frozen model. Another consequence of the mentioned phenomena would be the cone-shaped growth of the columns.
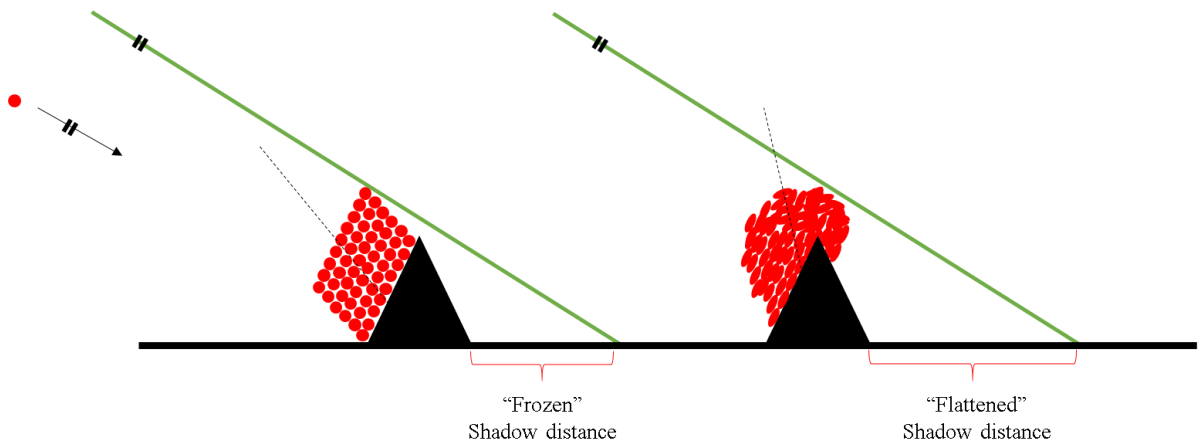
Figure 4-2: Column growth mechanism in frozen and flattened models and their effective shadow distance

4.1.2. Influence of substrate surface geometry on coating build-up

The review provided in Chapter two showed that the substrate roughness could have a deterministic effect on the microstructure of the coating. In this section, some substrate surface characteristics are studied systematically to provide a qualitative assessment of their impact.

Figure 4-3 shows the effect of substrate roughness, peak height 10 µm and 20 µm at a constant 50 µm peak-to-peak distance, on the coating evolution by the frozen and flattened models. In the 10 µm case with the frozen model, some columns start to grow in the middle of the asperities. In other words, in this specific case, the shadow distance initiated by the 10 µm peaks is not enough to control the growth of columns in a 50 µm space. The same trend is also seen in the flattened model. In the case of 20 µm roughness, the inter-columnar gaps are more defined, and the formation of

columns is more uniform as the influence of the shadow effect is larger as compared to the 10 μm roughness case.
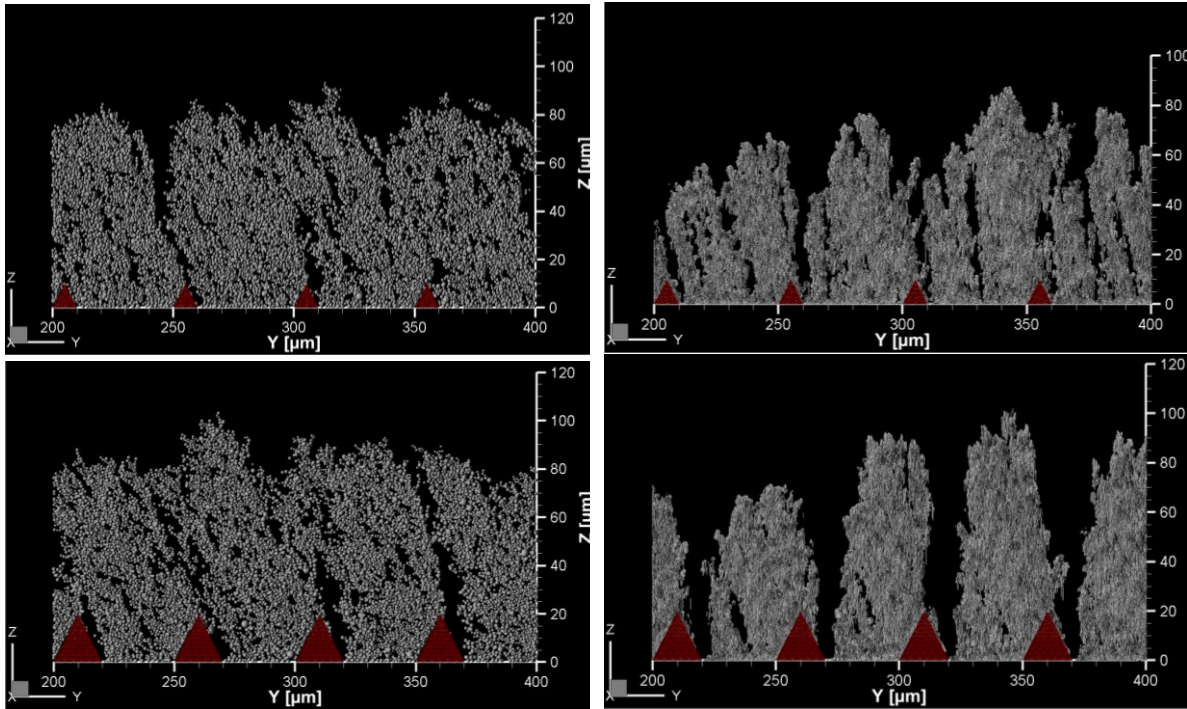
Figure 4-3: Simulation results showing the effect of roughness value on the coating microstructure by frozen (left) and flattened (right) models

Figure 4-4 represents the effect of peak-to-peak distance on the formation of columns. For this purpose, 10 μm roughness cones are put in 20 μm and 50 μm distance from each other. As mentioned before, in the case of 50 μm distance, some middle columns start to grow in between the peaks. By decreasing the distance to 20 μm, the shadow made by 10 μm peaks is enough to control the creation of the columns. Similar to other cases, the inter-columnar gaps remain more defined in the flattened model, while the coating characteristics are very close to the frozen model. As can be seen, a very uniform columnar microstructure is achieved in case of the 20 μm distance with the flattened model regarding orientation, width, and height of the columns.
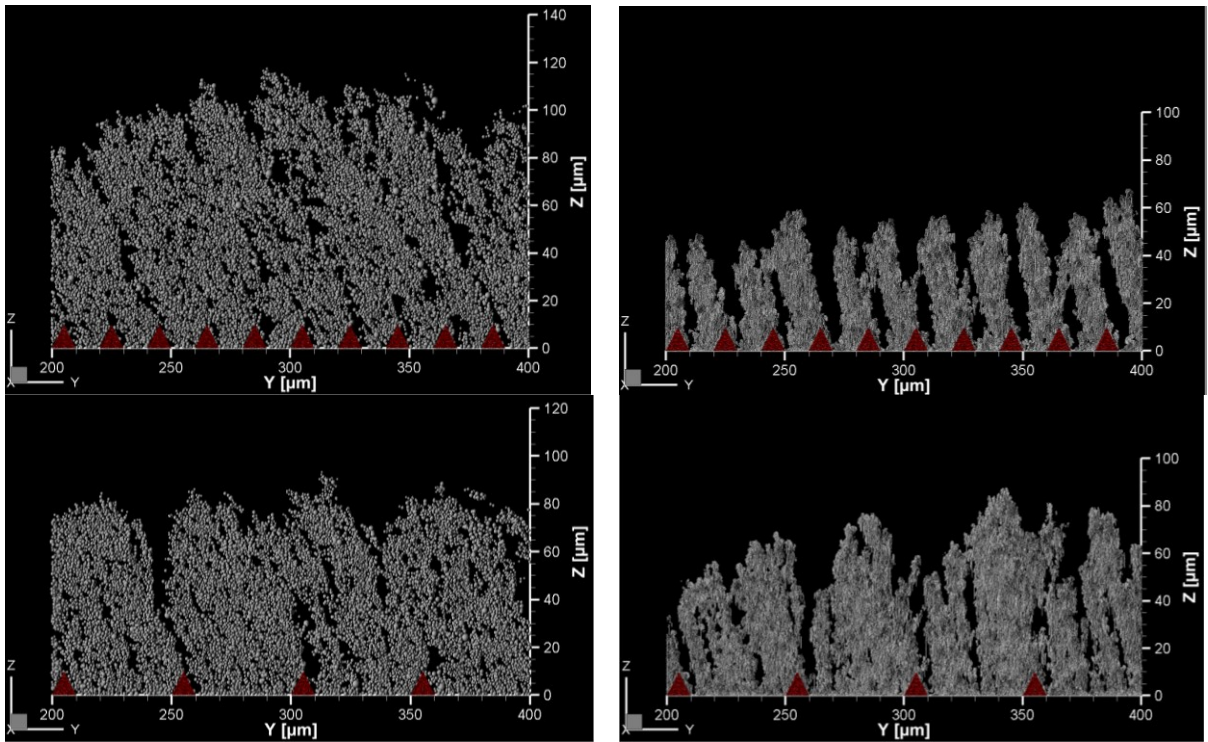
Figure 4-4: Simulation results showing the effect of peak-to-peak distance on the coating microstructure by frozen (left) and flattened (right) models

Figure 4-5 shows the effect of the roughness aspect ratio on the formation of the columns. By decreasing the aspect ratio, it is expected that the efficiency of a peak in initiating the growth of a column is reduced, and the coating is expected to show characteristics more similar to the smooth substrate. The results shown in Figure 4-5 show that, in the lower aspect ratio case with the frozen model, the microstructure does not follow the asperities at all, and a very non-uniform microstructure has formed. In the flattened model, also the gaps can be seen on both sides of the peaks, and the effect of asperities is lower compared to the case with the higher aspect ratio.
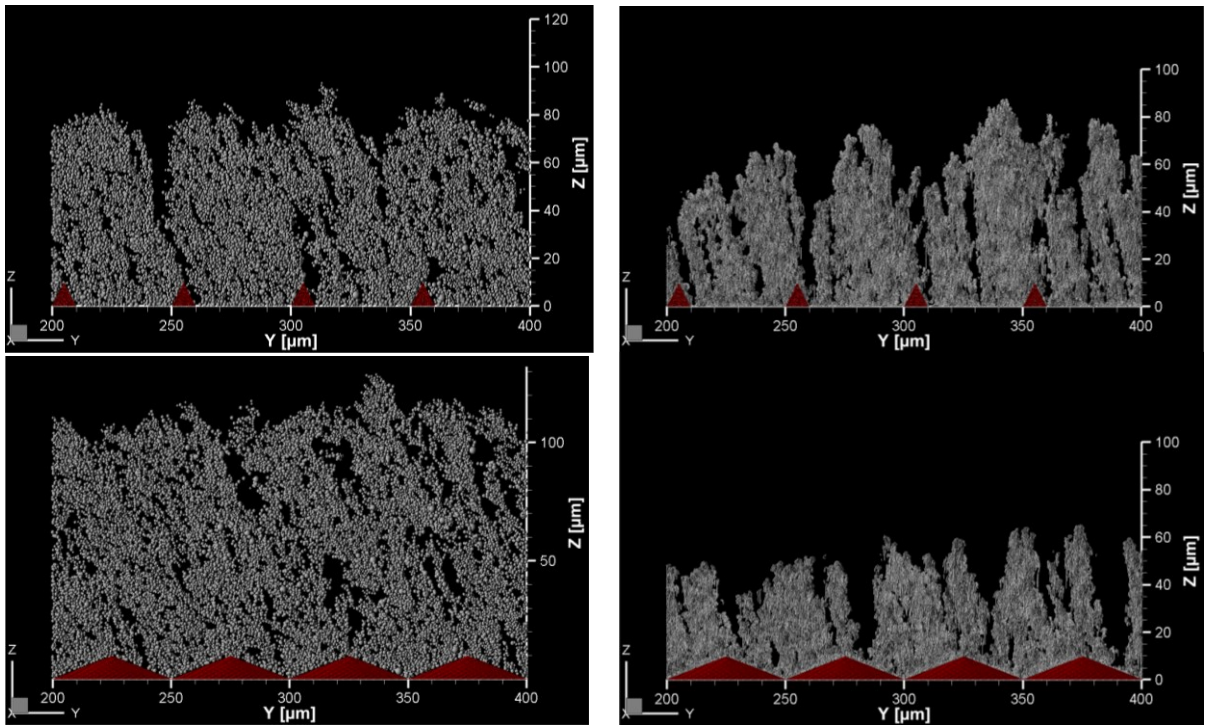
Figure 4-5: Simulation results showing the effect of cone asperities aspect ratio on the coating microstructure by frozen (left) and flattened (right) models

The last discussion of this section is around the investigation of the formation of a coating on a non-uniform substrate to simulate what is seen in reality. For this purpose, a layer of coating with the frozen model was created, giving a random surface, followed by applying the flattened model to coat it. As can be seen in Figure 4-6, the columns are randomly distributed, but still keep the same characteristics such as ragged surface and columnar.
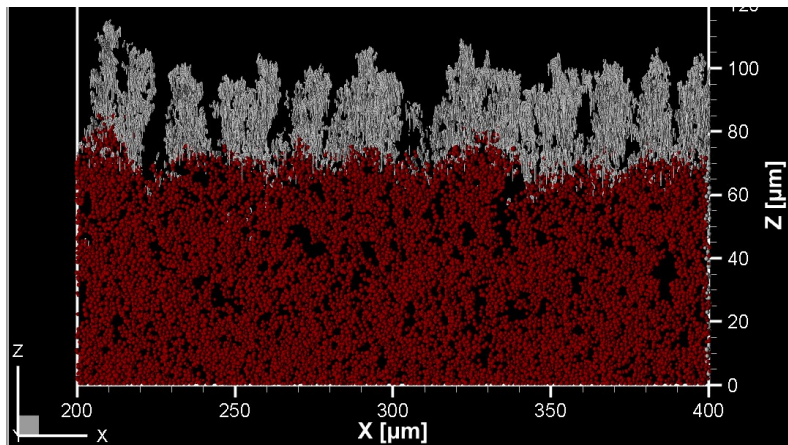
Figure 4-6: Application of frozen model (red) to provide a random surface coated by applying the flattened model (white)

4.1.3. Influence of flattening ratio on coating build-up

The effect of flattening ratio, as referred to by FR in previous chapter, is investigated in Figure 4-7. As can be seen, a vague columnar microstructure is observed in the frozen model, while by increasing the flattening ratio, the flattened models show columnar microstructure with a more defined interspace and ragged surface.
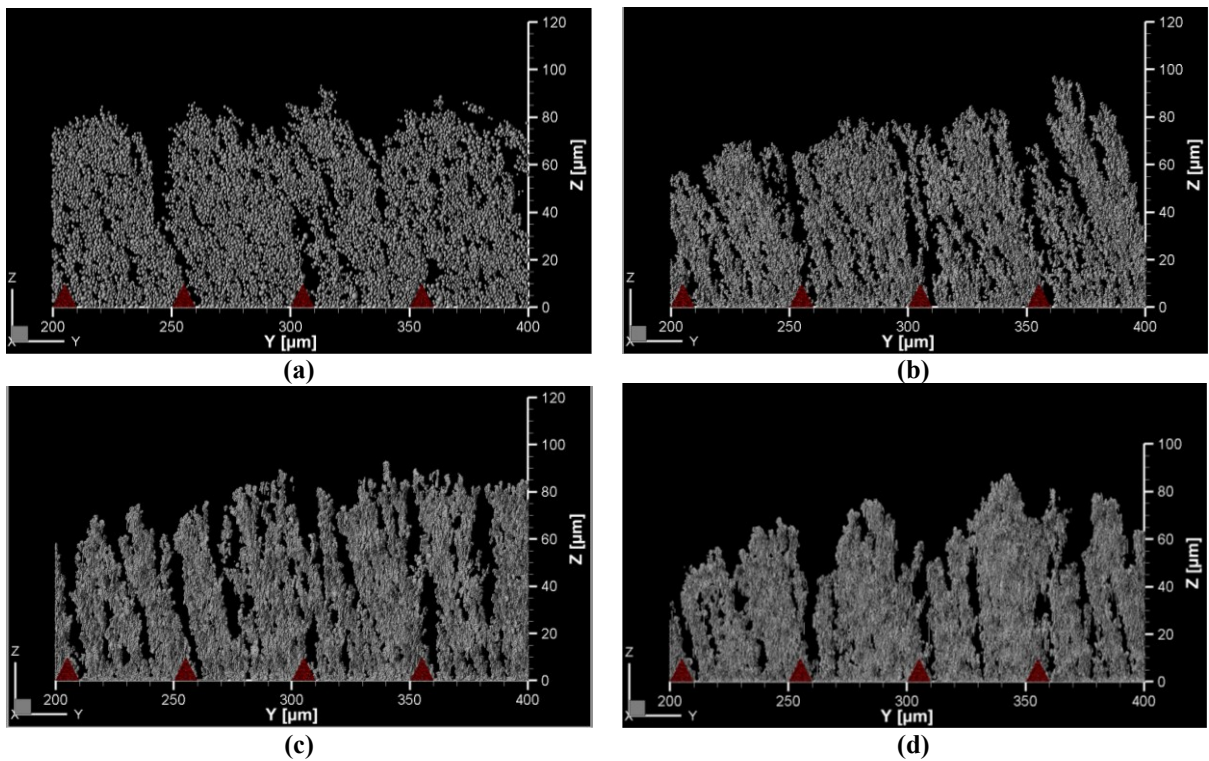
Figure 4-7: Effect of flattening ratio on the coating microstructure (a):1, (b):1.5, (c):2, (d):3

1.1.3. Influence of particle trajectory on coating build-up

The shadow effect explained in the first chapter was identified as the main mechanism behind the formation of columnar microstructure in SPS coatings. Two essential components making the shadow effect are the angle of the particle trajectories relative to substrate level, and local peaks on the coated surface.

In the results presented below, the z component of particle velocity was multiplied in four to provide particles with a more perpendicular trajectory upon impact. Figure 4-8 shows the results of the coating build-up from the frozen and flattened models, where a roughened substrate was applied, as the worst case, to enhance the formation of columns. As can be seen in both models, even despite the enhancement of the potential for columnar growth, the coating columnar characteristics has been reduced noticeably compared to the original distribution showed in Figure 4-4. In fact, the coating has filled all the space around asperities and the non-uniformity of substrate surface has been made even by the coating build-up. This observation is compatible with the shadow effect theory, as the perpendicular particles cannot make a shadow.
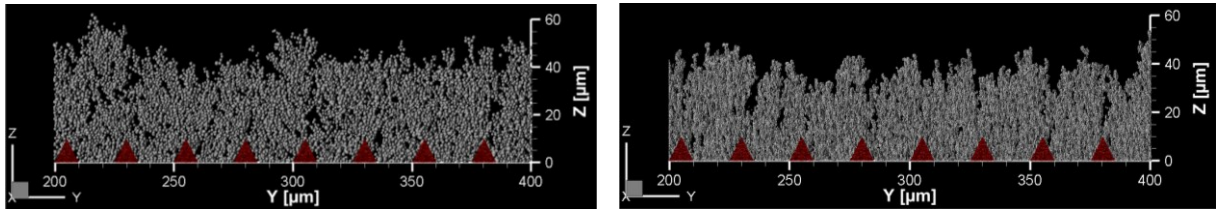
Figure 4-8: Simulation results for perpendicular impact by frozen (left) and flattened (right) models

In the second part of this section, the z-component of particle velocity was divided by three, making particle trajectory with shallower impact angles. The results of the study are shown in Figure 4-9 for the frozen and flattened models, while a smooth substrate was considered to weaken the formation of columns. As can be seen, despite weakening the potential for the formation of columns, both models predict a highly columnar microstructure. These coating are more porous compared to the original case, as shown in Figure 4-1, which is believed to be due to stronger shadow effect coming from shallower trajectories, leading to higher intercolumnar spaces. As was seen previously, this study also the flattened model predicts wider inter-columnar space compared to the frozen model. It should be mentioned that in the current results, the orientation of columns

predicted by the frozen model is more inclined compared to the original case. In contrast, the flattened model shows no significant changes in this regard.
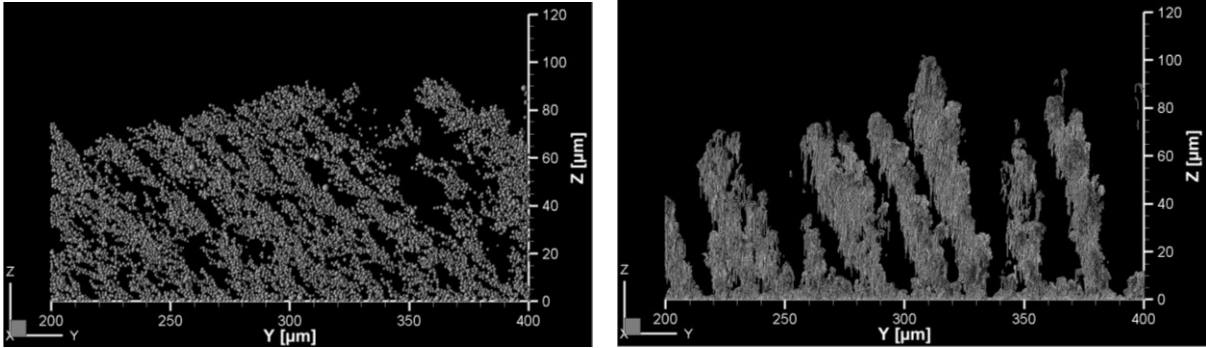
Figure 4-9: Simulation results for accentuated shallow impact by frozen (left) and flattened (Right) models

In the third case, the torch configuration 1, sweeping a linear pattern with 3 mm interspaces, was applied along with the original particle trajectory. In this case, the frozen model predicts a feather-like columnar microstructure as reported in the literature, while the It should be mentioned that regardless of keeping the original trajectory, by making the interested area closer to the torch axis, the landing particles would have a more perpendicular impact compared to configuration-2. Figure 4-10 shows the results of frozen and flattened models. The frozen model shows the formation of a microstructure called "feather-like" on top of the asperities. In contrast, the flattened model, as was seen previously, shows no sensitivity to the particle trajectory.
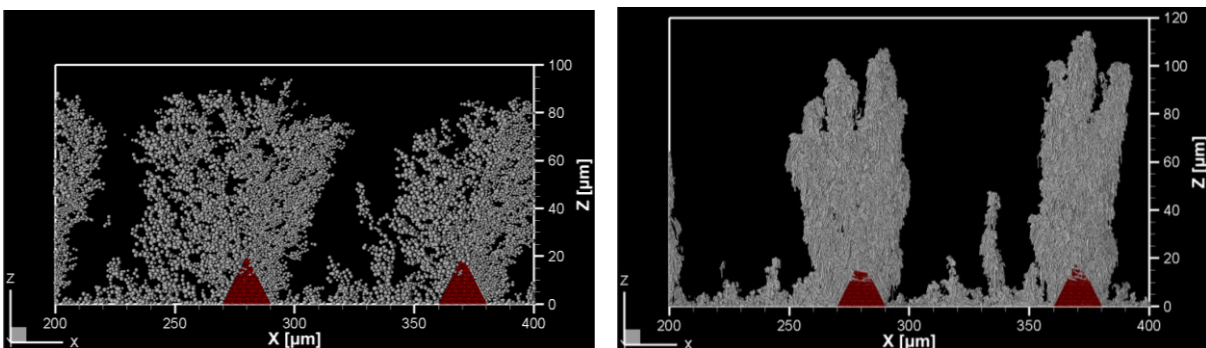
Figure 4-10: Formation of "feather-like" microstructure in frozen model, while flattened model shows no sensitivity to the particle trajectory

1.2. Result for the full-raster torch sweeping

In this section, the evolution of coating build-up with the torch sweeping a full-raster is studied, which conceptually allows the deposition of a more extensive variety of the particles. This part of study focuses on the differences between full-raster and linear-raster, the effect of substrate geometry and torch speed on the coating microstructure.

1.2.1. Coating build-up on smooth substrate

The microstructures of coatings deposited on a smooth substrate by the frozen and flattened models are compared in Figure 4-11. Similar to the linear-raster cases, the microstructure is columnar, while the space between columns is widened in this case. This observation could be justified based on the fact that the shadow made by a peak in full-raster case covers an area all around it, while just a part of that area would be covered in the case of linear-raster.
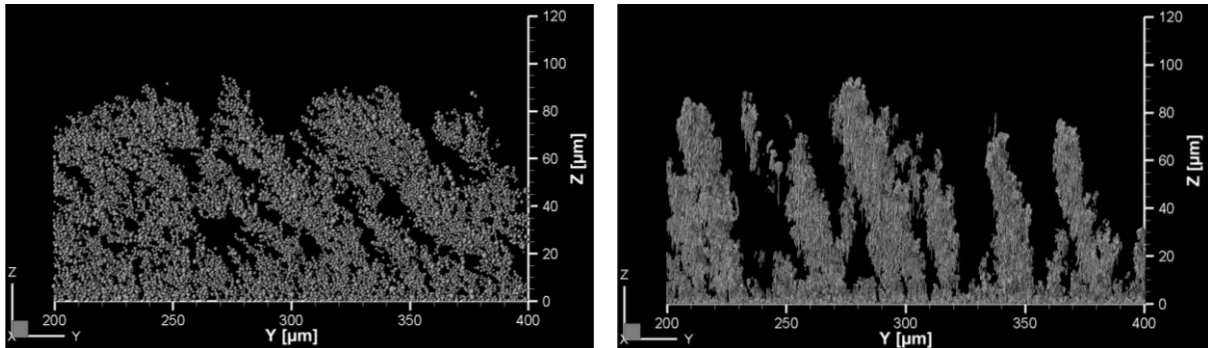
Figure 4-11: Coating morphology by frozen (left) and flattened (right) models in full-raster

It should be mentioned that the difference between frozen and flattened models is the same as what explained in the linear-raster case; therefore, the continuation of the study will focus on the results from the more general flattened model.

1.2.2. Influence of substrate geometry on coating build-up

Figure 4-12 shows the evolution of coating in the case of the substrate of 10 µm roughness in a peak-to-peak distance of 50 µm and 20 µm by flattened model. In the case of 50 µm distance,

the columns are broader and more defined, while the other case provides thinner columns that grew

unevenly with a narrower inter-space. Comparing those results with a similar case in linear-raster

as was shown in Figure 4-4, the interspace between columns has widened, and the coating has a

more uneven surface.

Based on the set of particle distribution shown in Figure 3-4, the linear-case configuration-

2, sweeping the middle of the modelled, was adjusted to provide the highest number of particles

around the modeled area. This extensivity leads to a more uniform deposition, which is probably

the reason for more even coating surface in linear-raster case.
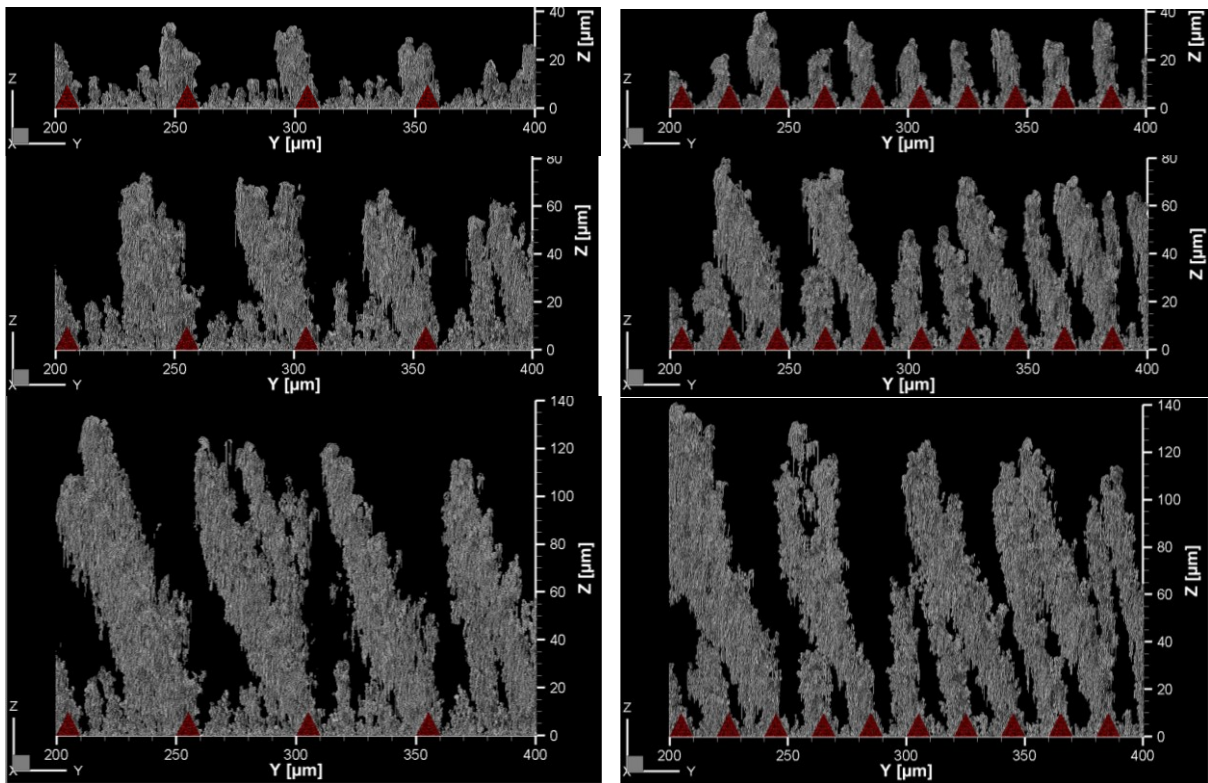
Figure 4-12: Coating evolution in case of 10 μm roughness in peak-to-peak distances of 50 μm (left)
and 20 μm for 7, 14, and 28 passes (right)

Based on these obtained results, it was tried to build a microstructure which has the evenness of

the 50 μm case and the thin intercolumn space of the 10 μm peak-to-peak distance. Therefore, the

peak-to-peak distance was set on 35 μm, the average of the two cases. The results of the three trials

are compared in Figure 4-10 showing a view of the coatings cut on a cross-section that includes the roughness peaks, and the top view of the coating surface. As can be seen, the 35 µm has heritage from both models.
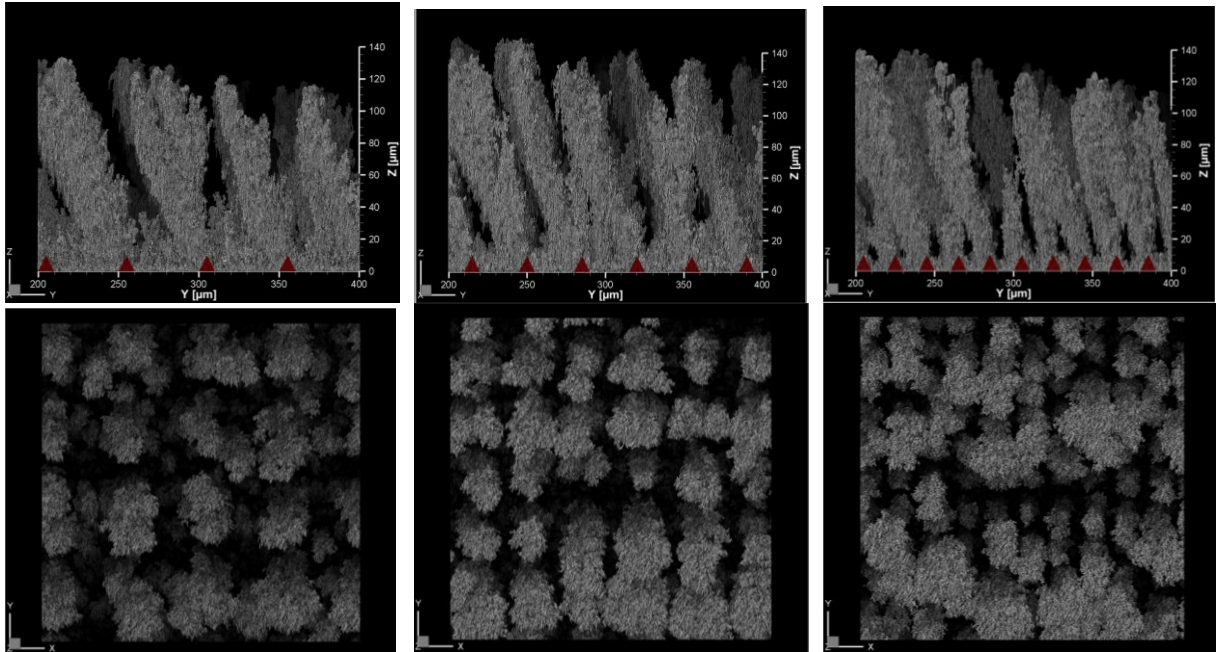
Figure 4-13: Final coating microstructure cross-section (up) and surface (down) view for the case of 10 µm roughness in peak-to-peak distances of 50 µm (left) and 20 µm (middle) and 35 µm (right)

1.2.3. Influence of torch speed on coating build-up

Based on Bernard et al. [23] investigations, as reviewed in chapter two, increasing torch speed is expected to uniform the microstructure of the coating. The results of a 50% decrease and increase of torch speed are shown in Figure 4-14 compared to the original speed. The results show the top view of a 10 µm thick cross-section of coating parallel to the substrate plane from 20 µm to 30 µm in (a, b, c), and from 60 µm to 70 µm in (d, e, f). It must be mentioned that this specific representation would be advantageous as the distribution of columns are supposed to be compared on the whole substrate. As shown in Figure 4-14, it seems that comparing case (a) with (b), and (c), the columns are narrower and intercolumnar spaces are wider. However, after the growing and

intersect of columns, the coating growth does not follow the initial substrate coming from

embedded asperities, as shown in cases of (d), (e) and (f).

<table>
<tr><td>(a)</td><td>(b)</td><td>(c)</td></tr>
<tr><td>(d)</td><td>(e)</td><td>(f)</td></tr>
</table>
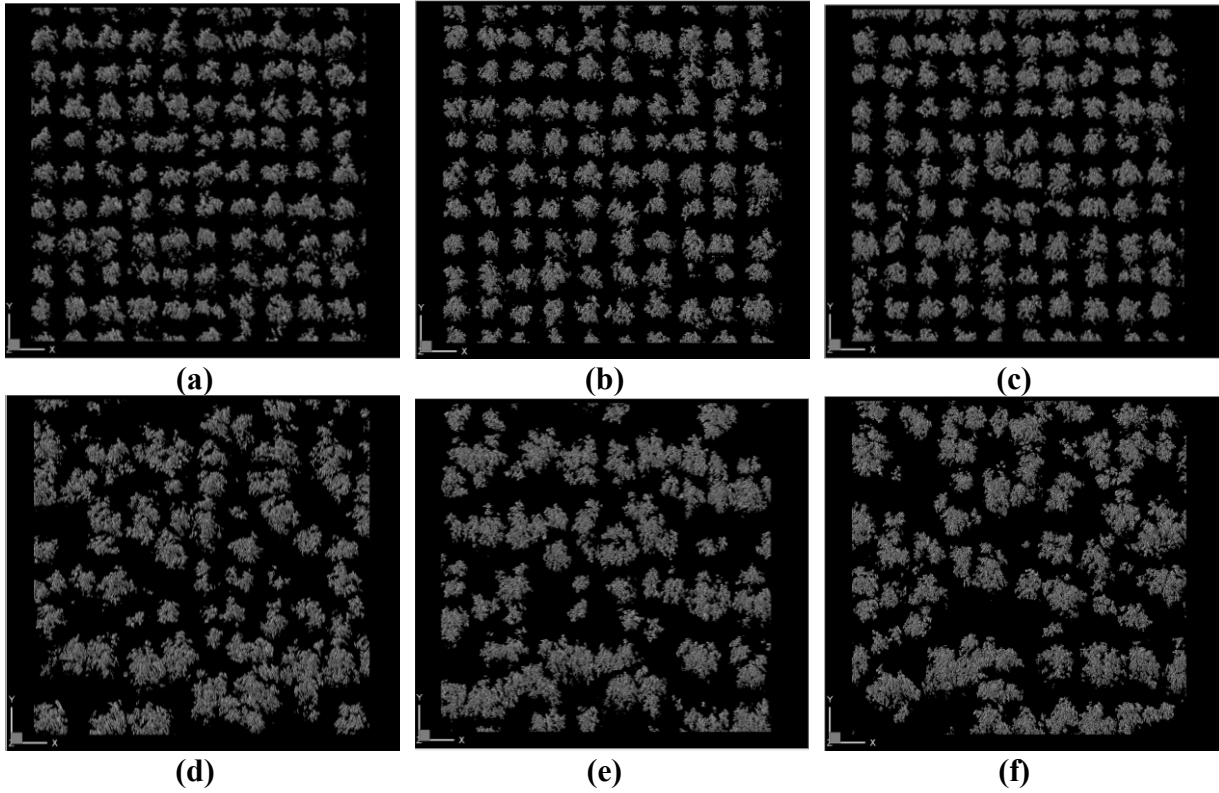
Figure 4-14: Cross-section of the coating parallel to substrate with 10-µm substrate roughness at peak-to-peak distances of 20 µm with 0.5 m/s (a, d), 1 m/s (b, e) and 1.5 m/s (c, f) torch speed

Conclusion and Future works

The procedure of developing an SPS coating build-up simulation tool was described. For this purpose, the distribution of particles at 100 µm distance relative to the substrate was taken from the CFD simulations [3], and some assumptions were made considering the flying particle trajectory and the splat formation. The flying particle trajectory was assumed not to vary till deposition, and two theories regarding the splat geometry were introduced. The first model considered the deposition as a solid material, called the frozen model, while the second model considered a splat geometry similar to a kite, depending on the flying particle trajectory.

The results from the two models showed some similar coating characteristics such as the type of microstructure and number of columns. However, there were considerable differences of the porosity, intercolumnar spaces and coating surface roughness. Generally, the developed tool provides promising results compared to the trends already reported in the open literature, such as the effect of substrate roughness on the formation of columns. However, due to the lack of CFD results, it was not possible to perform a comprehensive study regarding the effect of plasma flow variables on the coating microstructure.

The simulation process still has some elements which need to be improved in the future. The plasma fluctuations should be seen in CFD simulations and a larger substrate should be applied to simulate the reality. Regarding the developed tool, the following problems should be addressed:

1. **Overpredicting deposition rate and porosity level**: both frozen and flattened models predict a porous microstructure. Applying spheres in forming the splat morphology, and lack of diversity in the flying particles dataset could be mentioned as the main reasons. This overprediction of porosity also leads to overprediction of deposition rate. However, a part of this problem comes from neglecting the rebound effect.

2. **Curved trajectory**: lighter particles experience major change of trajectory before deposition. Providing a model relating the particle size and deposition angle could lead to a more realistic prediction of the coating build-up simulation.

From the programming standpoint, it should be mentioned that the running speed is a function of coating thickness, due to the higher number of particles processed. However, this problem could be addressed by assuming a penetration depth and ignoring the underlying particles. Parallel computation is also an applicable choice to boost the running speed, as the substrate area has already been divided into smaller computational areas to be distributed between the CPUs.

[1]   K. O. Legg, M. Graham, P. Chang, F. Rastagar, A. Gonzales, and B. Sartwell, "The replacement of electroplating," *Surf. Coatings Technol.*, vol. 81, no. 1, pp. 99–105, May 1996, doi: 10.1016/0257-8972(95)02653-3.

[2]   S. Ghafouri Azar, "Three-Dimensional Simulation of Coating Build-up In Suspension Plasma Spray Process," Concordia University, 2018.

[3]   K. Pourang, C. Moreau, and A. Dolatabadi, "Effect of Substrate and Its Shape on in-Flight Particle Characteristics in Suspension Plasma Spraying," *J. Therm. Spray Technol.*, vol. 25, no. 1–2, pp. 44–54, Jan. 2016, doi: 10.1007/s11666-015-0342-z.

[4]   C. J. Li, "Thermal spraying of light alloys," in *Surface Engineering of Light Alloys: Aluminium, Magnesium and Titanium Alloys*, Elsevier Inc., 2010, pp. 184–241.

[5]   N. Krishnan, A. Vardelle, and J. Legoux, "A life cycle comparison of hard chrome and thermal sprayed coatings : a case example of aircraft landing gears," *Int. Therm. Spray, ITSC 2008, Therm. Spray Crossing Borders*, Jun. 2008.

[6]   K. Yao, S. Chen, K. Guo, C. K. I. Tan, M. S. Mirshekarloo, and F. E. H. Tay, "Lead-Free Piezoelectric Ceramic Coatings Fabricated by Thermal Spray Process," *IEEE Trans. Ultrason. Ferroelectr. Freq. Control*, vol. 64, no. 11, pp. 1758–1765, Nov. 2017, doi: 10.1109/TUFFC.2017.2748154.

[7]   M. Jadidi, M. Mousavi, S. Moghtadernejad, and A. Dolatabadi, "A Three-Dimensional Analysis of the Suspension Plasma Spray Impinging on a Flat Substrate," *J. Therm. Spray Technol.*, vol. 24, no. 1–2, pp. 11–23, Oct. 2014, doi: 10.1007/s11666-014-0166-2.

[8]   J. Oberste-Berghaus, *Injection conditions and in-flight particle states in suspension plasma spraying of alumina and zirconia nano-ceramics*. [Boucherville Quebec]: [National Research Council Canada Industrial Materials Institute], 2004.

[9]   P. L. Fauchais, J. V. R. Heberlein, and M. I. Boulos, *Thermal spray fundamentals : from powder to part*. Springer US, 2014.

[10]   A. Rico, J. Rodríguez, and E. Otero, "High temperature oxidation behaviour of nanostructured alumina-titania APS coatings," *Oxid. Met.*, vol. 73, no. 5–6, pp. 531–550, Jun. 2010, doi: 10.1007/s11085-010-9191-9.

[11]   F. Miranda, F. Caliari, A. Essiptchouk, and G. Pertraconi, "Atmospheric Plasma Spray Processes: From Micro to Nanostructures," in *Atmospheric Pressure Plasma - from Diagnostics to Applications*, IntechOpen, 2019.

[12]   P. Fauchais, "Understanding plasma spraying," *Journal of Physics D: Applied Physics*, vol. 37, no. 9. 07-May-2004, doi: 10.1088/0022-3727/37/9/R02.

[13]   S. Mahade, K. Narayan, S. Govindarajan, S. Björklund, N. Curry, and S. Joshi, "Exploiting Suspension Plasma Spraying to Deposit Wear-Resistant Carbide Coatings," *Materials (Basel).*, vol. 12, no. 15, p. 2344, Jul. 2019, doi: 10.3390/ma12152344.

[14]   Y. Bai, S. jian Zhou, L. Shi, W. Ma, and C. wen Liu, "Fabrication and Characterization of Suspension Plasma-Sprayed Fluoridated Hydroxyapatite Coatings for Biomedical

Applications," *J. Therm. Spray Technol.*, vol. 27, no. 8, pp. 1322–1332, Dec. 2018, doi: 10.1007/s11666-018-0747-6.

[15]   W. Fan and Y. Bai, "Review of suspension and solution precursor plasma sprayed thermal barrier coatings," *Ceramics International*, vol. 42, no. 13. Elsevier Ltd, pp. 14299–14312, 01-Oct-2016, doi: 10.1016/j.ceramint.2016.06.063.

[16]   N. Curry, K. VanEvery, T. Snyder, and N. Markocsan, "Thermal Conductivity Analysis and Lifetime Testing of Suspension Plasma-Sprayed Thermal Barrier Coatings," *Coatings*, vol. 4, no. 3, pp. 630–650, Aug. 2014, doi: 10.3390/coatings4030630.

[17]   M. Gupta, *Design of Thermal Barrier Coatings. A Modelling Approach*, no. 3. Springer International Publishing, 2010.

[18]   K. VanEvery, M. J. M. Krane, R. W. Trice, H. Wang, and W. Porter, "Column formation in suspension plasma-sprayed coatings and resultant thermal properties," *J. Therm. Spray Technol.*, vol. 20, no. 4, pp. 817–828, Jun. 2011, doi: 10.1007/s11666-011-9632-2.

[19]   R. Rampon, O. Marchand, C. Filiatre, and G. Bertrand, "Influence of suspension characteristics on coatings microstructure obtained by suspension plasma spraying," *Surf. Coatings Technol.*, vol. 202, no. 18, pp. 4337–4342, Jun. 2008, doi: 10.1016/j.surfcoat.2008.04.006.

[20]   B. Bernard, A. Quet, L. Bianchi, A. Joulia, A. Malié, and V. Schick, "Thermal insulation properties of YSZ coatings: Suspension Plasma Spraying (SPS) versus Electron Beam Physical Vapor Deposition (EB-PVD) and Atmospheric Plasma Spraying (APS)," *Surf. Coatings Technol.*, vol. 318, pp. 122–128, May 2017, doi: 10.1016/j.surfcoat.2016.06.010.

[21]   D. Soysal and A. Ansar, "A new approach to understand liquid injection into atmospheric plasma jets," *Surf. Coatings Technol.*, vol. 220, pp. 187–190, Apr. 2013, doi: 10.1016/j.surfcoat.2012.12.009.

[22]   N. Curry, K. VanEvery, T. Snyder, J. Susnjar, and S. Bjorklund, "Performance testing of suspension plasma sprayed thermal barrier coatings produced with varied suspension parameters," *Coatings*, vol. 5, no. 3, pp. 338–356, 2015, doi: 10.3390/coatings5030338.

[23]   B. Bernard, L. Bianchi, A. Malié, A. Joulia, and B. Rémy, "Columnar suspension plasma sprayed coating microstructural control for thermal barrier coating application," *J. Eur. Ceram. Soc.*, vol. 36, no. 4, pp. 1081–1089, Mar. 2016, doi: 10.1016/j.jeurceramsoc.2015.11.018.

[24]   P. Sokołowski, L. Pawtowski, D. Dietrich, T. Lampke, and D. Jech, "Advanced microscopic study of suspension plasma sprayed zirconia coatings with different microstructures," in *Proceedings of the International Thermal Spray Conference*, 2015, vol. 1, pp. 1–8, doi: 10.1007/s11666-015-0310-7.

[25]   P. Kromer, P. Sokołowski, J. T. C. Rolando, S. Costil, and L. Pawlowski, "SPS coating microstructure controlled by the surface topography using laser texturing," in *Conference: International Thermal Spray Conference (ITSC)*, 2017.

[26] N. Curry, Z. Tang, N. Markocsan, and P. Nylén, "Influence of bond coat surface roughness on the structure of axial suspension plasma spray thermal barrier coatings - Thermal and lifetime performance," *Surf. Coatings Technol.*, vol. 268, pp. 15–23, Apr. 2015, doi: 10.1016/j.surfcoat.2014.08.067.

[27] P. Sokołowski, S. Kozerski, L. Pawłowski, and A. Ambroziak, "The key process parameters influencing formation of columnar microstructure in suspension plasma sprayed zirconia coatings," *Surf. Coatings Technol.*, vol. 260, pp. 97–106, Dec. 2014, doi: 10.1016/j.surfcoat.2014.08.078.

[28] R. Chidambaram Seshadri, G. Dwivedi, V. Viswanathan, and S. Sampath, "Characterizing Suspension Plasma Spray Coating Formation Dynamics through Curvature Measurements," *J. Therm. Spray Technol.*, vol. 25, no. 8, pp. 1666–1683, Dec. 2016, doi: 10.1007/s11666-016-0460-2.

[29] P. Wang, W. He, G. Mauer, R. Mücke, and R. Vaßen, "Monte Carlo simulation of column growth in plasma spray physical vapor deposition process," *Surf. Coatings Technol.*, vol. 335, pp. 188–197, Feb. 2018, doi: 10.1016/j.surfcoat.2017.12.023.

[30] K. Yang, M. Liu, K. Zhou, and C. Deng, "Recent Developments in the Research of Splat Formation Process in Thermal Spraying," *J. Mater.*, vol. 2013, pp. 1–14, Dec. 2013, doi: 10.1155/2013/260758.

[31] R. Nikbakht, S. H. Seyedein, S. Kheirandish, H. Assadi, and B. Jodoin, "Asymmetrical bonding in cold spraying of dissimilar materials," *Appl. Surf. Sci.*, vol. 444, pp. 621–632, Jun. 2018, doi: 10.1016/j.apsusc.2018.03.103.

[32] R. Ghafouri-Azar, J. Mostaghimi, S. Chandra, and M. Charmchi, "A stochastic model to simulate the formation of a thermal spray coating," *J. Therm. Spray Technol.*, vol. 12, no. 1, pp. 53–69, Mar. 2003, doi: 10.1361/105996303770348500.